

SPLITTING SCHEMES FOR A LAGRANGE MULTIPLIER FORMULATION OF FSI WITH IMMERSED THIN-WALLED STRUCTURE: STABILITY AND CONVERGENCE ANALYSIS

MICHELE ANNESE, MIGUEL A. FERNÁNDEZ, AND LUCIA GASTALDI

ABSTRACT. The numerical approximation of incompressible fluid-structure interaction problems with Lagrange multiplier is generally based on strongly coupled schemes. This delivers unconditional stability but at the expense of solving a computationally demanding coupled system at each time-step. For the case of the coupling with immersed thin-walled solids, we introduce a class of semi-implicit coupling schemes which avoids strongly coupling without compromising stability and accuracy. A priori energy and error estimates are derived. The theoretical results are illustrated through numerical experiments in an academic benchmark. fluid-structure interaction, immersed boundary method, Lagrange multiplier, finite elements, time-splitting schemes.

1. INTRODUCTION

The numerical simulation of multi-physics systems coupling an incompressible viscous fluid with an immersed thin-walled elastic solid is of major importance in many engineering and living systems. Among the examples, we can mention the aeroelasticity of parachutes and sailing boats and the mechanics of capsules, biological cells and heart valves (see, e.g., [46, 56, 28, 50, 53, 39, 48, 57]).

These coupled problems often feature large interface displacements, with potential contact between solids, so that the favored spatial discretization is mainly based on unfitted mesh approximations (the fluid mesh is not fitted to the fluid-solid interface). Among these methods, the most popular are the immersed boundary method (see, e.g., [52, 49, 10]) and the fictitious domain method (see, e.g., [37, 6, 27, 4, 42, 17, 2, 14, 25]), which treat the solid in its natural Lagrangian formalism. We refer to [19] for a recent numerical study which compares some of these approaches.

Over the last decade, significant advances have been achieved in the development and the analysis of time splitting schemes that avoid strong coupling without compromising stability and accuracy. The majority of these studies is limited to fitted fluid and solid meshes (see, e.g., [33, 54, 7, 23, 38, 22, 47, 32, 35, 8, 36, 34, 45]). Within the unfitted mesh framework, splitting schemes which efficiently avoid strong coupling are much more rare. The original time-stepping scheme of the immersed boundary method uncouples the fluid and solid time-marchings (actually, the solid solver is never called) but at the price of enforcing severe time-step restrictions for stability (see, e.g., [10]). The splitting schemes reported in [24, 2, 43, 41] are also known to enforce severe time-step restrictions for stability/accuracy or to be sensitive to the amount of added-mass effect.

In the present paper, we introduce a semi-implicit coupling scheme for a formulation based on the introduction of a Lagrange multiplier which avoids the above mentioned issues. The proposed approach generalizes the ideas introduced in [29, 31] to the case of unfitted mesh approximations with Lagrange multipliers (see [12, 14]). The analysis shows, in particular, that the scheme with first-order extrapolation yields unconditional stability and optimal (first-order) accuracy in time. To the best of our knowledge, this is the first time that the full numerical analysis is addressed for linear incompressible fluid-structure interaction problems with Lagrange multipliers. Numerical experiments in an academic test case illustrate the behavior of the proposed approach.

The rest of the paper is organized as follows. Section 2 presents the coupled system and its weak formulation with Lagrange multipliers. The numerical methods are described in Section 3. Section 4 presents the stability and the error analysis. Numerical evidence of the theoretical findings is provided in Section 5.

2. PROBLEM SETTING AND WEAK FORMULATION

We consider fluid-structure interaction problems characterized by a thin-walled structure immersed in an incompressible viscous fluid. Let $\Omega \subset \mathbb{R}^d$, $d = 2, 3$, be a fixed bounded domain with Lipschitz continuous boundary Γ . In order to describe the dynamics of the structure immersed in the fluid, we use a Lagrangian framework. The elastic thin-walled structure is represented by its mid-surface (i.e., a curve if $d = 2$ or a surface if $d = 3$). Let $\Sigma \subset \mathbb{R}^d$ be the reference configuration of the thin-walled structure mid-surface. Its current position, denoted by $\Sigma(t)$, is obtained as the image of the deformation mapping $\phi(\cdot, t) : \Sigma \rightarrow \Sigma(t) \subset \Omega$. The domain occupied by the fluid is denoted $\Omega(t) = \Omega \setminus \Sigma(t)$ and its boundary by $\partial\Omega(t) = \Gamma \cup \Sigma(t)$. We assume that the interface $\Sigma(t)$ is oriented by a unitary normal vector field \mathbf{n} , which induces a positive and a negative side in the fluid domain $\Omega(t)$, with respective unit normals $\mathbf{n}^+ := \mathbf{n}$ and $\mathbf{n}^- := -\mathbf{n}$ on $\Sigma(t)$. Thus, we can define the positive and negative sided-restrictions to $\Sigma(t)$ of a given field f defined in $\Omega(t)$, as $f^+(\mathbf{x}) := \lim_{\xi \rightarrow 0^+} f(\mathbf{x} + \xi \mathbf{n}^+)$, $f^-(\mathbf{x}) := \lim_{\xi \rightarrow 0^-} f(\mathbf{x} + \xi \mathbf{n}^-)$, $\forall \mathbf{x} \in \Sigma(t)$, and the normal jump $[[f\mathbf{n}]] := f^+ \mathbf{n}^+ + f^- \mathbf{n}^-$.

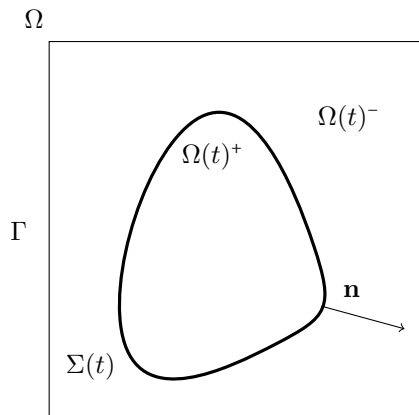


FIGURE 1. Geometrical configuration of the FSI problem.

We adopt the Eulerian framework to write the Navier-Stokes equations which govern the dynamics of the incompressible fluid and the Lagrangian framework for the elastodynamics of the thin structure. We denote by $\boldsymbol{\sigma}^f := -p\mathbb{I} + 2\mu\boldsymbol{\epsilon}(\mathbf{u})$ the Cauchy stress tensor for incompressible fluids, where $\boldsymbol{\epsilon}(\mathbf{u}) := (\nabla \mathbf{u} + \nabla \mathbf{u}^\top)/2$ is the strain tensor. We assume that the abstract linear surface differential operator \mathbf{L} describes the solid elastic effects. Hence, we have the following coupled problem.

Problem 1. *Given \mathbf{u}_0 , \mathbf{d}_0 and \mathbf{d}_1 , for $t \in]0, T]$, find the fluid velocity \mathbf{u} , the pressure p in $\Omega(t)$, the solid displacement \mathbf{d} and velocity $\dot{\mathbf{d}}$ in Σ such that:*

• **Fluid sub-problem:**

$$(1) \quad \begin{cases} \rho^f (\partial_t \mathbf{u} + \mathbf{u} \nabla \mathbf{u}) - \operatorname{div} \boldsymbol{\sigma}^f = \mathbf{0} & \text{in } \Omega(t), \\ \operatorname{div} \mathbf{u} = 0 & \text{in } \Omega(t), \\ \mathbf{u} = \mathbf{0} & \text{on } \Gamma. \end{cases}$$

• **Solid sub-problem:**

$$(2) \quad \begin{cases} \rho^s \varepsilon \partial_t \dot{\mathbf{d}} + \mathbf{L} \mathbf{d} = \mathbf{f}_\Sigma & \text{in } \Sigma, \\ \partial_t \mathbf{d} = \dot{\mathbf{d}} & \text{in } \Sigma, \\ \mathbf{d} = \mathbf{0} & \text{on } \partial \Sigma. \end{cases}$$

• **Interface coupling conditions:**

$$(3) \quad \begin{cases} \phi = \mathbf{I} + \mathbf{d} & \text{in } \Sigma, \\ \mathbf{u} \circ \phi = \dot{\mathbf{d}} & \text{on } \Sigma, \\ \int_\Sigma \mathbf{f}_\Sigma \cdot \mathbf{w} = - \int_{\Sigma(t)} \llbracket \boldsymbol{\sigma}^f \mathbf{n} \rrbracket \cdot \mathbf{w} \circ \phi_t^{-1} & \forall \mathbf{w} : \Sigma \rightarrow \mathbb{R}^d \text{ smooth.} \end{cases}$$

• **Initial conditions:**

$$(4) \quad \begin{cases} \mathbf{u}(\cdot, 0) = \mathbf{u}_0 & \text{in } \Omega(0), \\ \mathbf{d}(\cdot, 0) = \mathbf{d}_0, \quad \dot{\mathbf{d}}(\cdot, 0) = \mathbf{d}_1 & \text{in } \Sigma. \end{cases}$$

The relation (3)₂ enforces the so-called kinematic coupling condition (continuity of velocity across the interface), while (3)₃ states that the tractions along the immersed interface have to be equilibrated (dynamic coupling).

Remark. In Problem 1, the solid mid-surface is fully identified with the fluid-solid interface Σ , by neglecting the solid thickness effects in the interface coupling. This is a rather widespread modeling assumption when coupling thin-walled solids with a 3D media (see, e.g., [26, 44]). Yet, in the context of immersed boundary methods, a correction term is often introduced to remove the *across-the-thickness* additional fluid mass (see, e.g., [11, 12]).

In the following, we introduce the weak formulation of Problem 1. We shall make use of the standard Sobolev space $H_0^1(D)^d$ of the vector valued functions in $H^1(D)$ which vanish on the boundary Γ , and of $L_0^2(D)$ the subspace of functions in $L^2(D)$ with zero mean value in D . The corresponding norms are denoted by $\|\cdot\|_1$ and $\|\cdot\|_0$, respectively. The scalar product in $L^2(D)$ is denoted by $(\cdot, \cdot)_D$. The subscript is dropped if $D = \Omega$. We denote by $\mathbf{W} \subseteq H^1(\Sigma)^d$ the subspace of admissible deformation which satisfy the Dirichlet boundary condition for the solid. Moreover, we shall use the bilinear forms $a^f : (H_0^1(\Omega)^d \times L_0^2(\Omega)) \times (H_0^1(\Omega)^d \times L_0^2(\Omega)) \rightarrow \mathbb{R}$

solving at each time step a high-dimensional heterogenous system, which can be ill conditioned and computational demanding.

3.2.2. Splitting schemes. In order to circumvent the computational complexity of the strong coupling (Algorithm 1), the time discretizations of the original immersed boundary method introduced a significant time splitting in the computation of the fluid and solid fields (see, e.g., [51, 58]). Basically, the idea consisted in treating explicitly the solid elastic contributions within the fluid and then retrieving the solid displacement directly from the interpolation of the fluid velocity into the solid grid. The fundamental drawback of this approach is that restrictive CFL-like conditions are required for stability (see, e.g., [58, 55, 16, 15, 11]). Within the context of the spatial approximation provided by Problem 3, this solution procedure would take the following form:

Algorithm 2. Let $\mathbf{u}_{0,h} \in \mathbf{V}_h$, $\mathbf{d}_{0,h} \in \mathbf{W}_h$, $\mathbf{d}_{1,h} \in \mathbf{W}_h$ and $\phi_{0,h} \in \mathbf{W}_h$ be given. We set $\mathbf{u}_h^0 = \mathbf{u}_{0,h}$, $\mathbf{d}_h^0 = \mathbf{d}_{0,h}$ and $\dot{\mathbf{d}}_h^0 = \mathbf{d}_{1,h}$. For $n = 1, \dots, N$, perform the following steps:

$$(14) \quad \begin{aligned} & : \text{Step 1. Find } (\mathbf{u}_h^n, p_h^n, \boldsymbol{\lambda}_h^n, \dot{\mathbf{d}}_h^n) \in \mathbf{V}_h \times Q_h \times \boldsymbol{\Lambda}_h \times \mathbf{W}_h \text{ such that:} \\ & \left\{ \begin{array}{ll} \rho^f (\partial_\tau \mathbf{u}_h^n, \mathbf{v}) + b(\mathbf{u}_h^{n-1}, \mathbf{u}_h^n, \mathbf{v}) + a_h^f((\mathbf{u}_h^n, p_h^n), (\mathbf{v}, q)) \\ \quad + c(\boldsymbol{\lambda}_h^n, \mathbf{v} \circ \phi_h^{n-1}) - c(\boldsymbol{\mu}, \mathbf{u}_h^n \circ \phi_h^{n-1} - \dot{\mathbf{d}}_h^n) = 0 & \forall (\mathbf{v}, q, \boldsymbol{\mu}) \in \mathbf{V}_h \times Q_h \times \boldsymbol{\Lambda}_h, \\ \rho^s \varepsilon (\partial_\tau \dot{\mathbf{d}}_h^n, \mathbf{w})_\Sigma = c(\boldsymbol{\lambda}_h^n, \mathbf{w}) - a^s(\mathbf{d}_h^{n-1}, \mathbf{w}) & \forall \mathbf{w} \in \mathbf{W}_h. \end{array} \right. \\ & : \text{Step 2. Update solid displacement: } \mathbf{d}_h^n = \mathbf{d}_h^{n-1} + \tau \dot{\mathbf{d}}_h^n. \\ & : \text{Step 3. Update interface: } \phi_h^n = \mathbf{I} + \mathbf{d}_h^n. \end{aligned}$$

The main idea behind the splitting of Algorithm 2 is to treat separately the two forcing terms: the solid inertial and elastic contributions are, respectively, implicitly and explicitly coupled with the fluid. The first avoids added-mass stability issues while the second introduces a certain degree of splitting in the time-discretization. Note that, contrarily to Algorithm 1, the solid solver is never called in Algorithm 2. In fact, this is the source of instability in the scheme. Indeed, a simple argument shows that by testing (14) with $(\mathbf{v}, q, \boldsymbol{\mu}) = (\mathbf{u}_h^n, p_h^n, \boldsymbol{\lambda}_h^n)$ we get the energy estimate

$$(15) \quad \begin{aligned} & \rho^f \|\mathbf{u}_h^n\|_{0,\Omega}^2 + 4\mu \sum_{m=1}^N \tau \|\boldsymbol{\epsilon}(\mathbf{u}_h^m)\|_{0,\Omega}^2 + \rho^s \varepsilon \|\dot{\mathbf{d}}_h^n\|_{0,\Sigma}^2 + \|\mathbf{d}_h^n\|_s^2 + 2 \sum_{m=1}^N \tau |p_h^m|_{s_h}^2 \\ & \leq \rho^f \|\mathbf{u}_h^0\|_{0,\Omega}^2 + \rho^s \varepsilon \|\dot{\mathbf{d}}_h^0\|_{0,\Sigma}^2 + \|\mathbf{d}_h^0\|_s^2 + \|\mathbf{d}_h^0\|_s^2 + 2 \sum_{m=1}^N \tau a^s(\mathbf{d}_h^m - \mathbf{d}_h^{m-1}, \dot{\mathbf{d}}_h^m). \end{aligned}$$

Note that the last term is nothing but the artificial power generated by the explicit treatment of the solid elastic contributions in (14). This can be controlled, but at the expense of enforcing restrictive CFL-like stability conditions (see Remark 3.2.2 for the details).

Remark. In order to get stability from (15), the last term can be controlled via a Gronwall type argument. Indeed, it suffices to use the continuity of a^f and a

4.1. Energy stability analysis. This section is devoted to the analysis of the stability properties of Algorithm 3. To this purpose, we first recall some auxiliary results which will be used later. The first one is a quite general version of discrete Gronwall's Lemma from [40].

Lemma 1. *Let τ, B and a_m, b_m, c_m, γ_m , for integers $m \geq 1$, be non negative numbers such that, for $n \geq 1$*

$$a_n + \tau \sum_{m=1}^n b_m \leq \tau \sum_{m=1}^n \gamma_m a_m + \tau \sum_{m=1}^n c_m + B.$$

Suppose that $\tau\gamma_m < 1$ for all $m \geq 1$. Then, for $n \geq 1$ it holds

$$a_n + \tau \sum_{m=1}^n b_m \leq \exp\left(\tau \sum_{m=1}^n \frac{\gamma_m}{1 - \tau\gamma_m}\right) \left(\tau \sum_{m=1}^n c_m + B\right).$$

We define a discrete counterpart $\mathbf{L}_h : \mathbf{W} \rightarrow \mathbf{W}_h$ of the elastic operator \mathbf{L} as follows:

$$(19) \quad (\mathbf{L}_h \mathbf{w}, \mathbf{z})_\Sigma = a^s(\mathbf{w}, \mathbf{z})$$

for all $\mathbf{z} \in \mathbf{W}_h$. In [29, Lemma 1] the following properties of \mathbf{L}_h have been proved:

Lemma 2. *Let $\mathbf{Lw} \in L^2(\Sigma)^d$, then*

$$(20) \quad \|\mathbf{L}_h \mathbf{w}\|_{0,\Sigma} \leq C \|\mathbf{Lw}\|_{0,\Sigma}.$$

Under the assumption that the mesh \mathcal{S}_h is quasi-uniform, then there exists a positive constant C_1 such that for all $\mathbf{w}_h \in \mathbf{W}_h$ it holds true

$$(21) \quad \|\mathbf{L}_h \mathbf{w}_h\|_s \leq C_1 h_s^{-2} \|\mathbf{w}_h\|_s.$$

From equation (18) we obtain the following characterization of the intermediate value of the displacement velocity in terms of the solid velocity and displacement:

Lemma 3. *Let $\{(\mathbf{u}_h^n, p_h^n, \boldsymbol{\lambda}_h^n, \dot{\mathbf{d}}_h^{n-\frac{1}{2}}, \mathbf{d}_h^n, \dot{\mathbf{d}}_h^n)\}_{n \geq 1} \subset \mathbf{V}_h \times Q_h \times \boldsymbol{\Lambda}_h \times \mathbf{W}_h \times \mathbf{W}_h \times \mathbf{W}_h$ be given by Algorithm 3. We have*

$$(22) \quad \dot{\mathbf{d}}_h^{n-\frac{1}{2}} = \dot{\mathbf{d}}_h^n + \frac{\tau}{\rho^s \varepsilon} \mathbf{L}_h (\mathbf{d}_h^n - \mathbf{d}_h^{n*}).$$

Proof. By subtraction (18)₁ from (17)₂ we get

$$(23) \quad \frac{\rho^s \varepsilon}{\tau} (\dot{\mathbf{d}}_h^{n-\frac{1}{2}} - \dot{\mathbf{d}}_h^n, \mathbf{w})_\Sigma - a^s(\mathbf{d}_h^n - \mathbf{d}_h^{n*}, \mathbf{w}) = 0$$

for all $\mathbf{w} \in \mathbf{W}_h$. The relation hence follows by from the definition of the discrete elastic operator (19). \square

The energy estimate for Algorithm 3 is given in terms of the *discrete energy* E_h^n and of the *discrete dissipation* D_h^n defined, respectively, as

$$(24) \quad \begin{aligned} E_h^0 &= \rho^f \|\mathbf{u}_{0,h}\|_{0,\Omega}^2 + \rho^s \varepsilon \|\mathbf{d}_{1,h}\|_{0,\Sigma}^2 + \|\mathbf{d}_{0,h}\|_s^2, \\ E_h^n &= \rho^f \|\mathbf{u}_h^n\|_{0,\Omega}^2 + \rho^s \varepsilon \|\dot{\mathbf{d}}_h^n\|_{0,\Sigma}^2 + \|\mathbf{d}_h^n\|_s^2, \\ D_h^n &= \sum_{m=1}^n \tau (4\mu \|\boldsymbol{\epsilon}(\mathbf{u}_h^m)\|_{0,\Omega}^2 + 2|p_h^m|_{s_h}^2). \end{aligned}$$

The following theorem states that the splitting scheme is unconditionally stable for $r = 1$, while for $r = 2$ it is conditionally stable.

Theorem 1. Let $\{(\mathbf{u}_h^n, p_h^n, \boldsymbol{\lambda}_h^n, \dot{\mathbf{d}}_h^{n-\frac{1}{2}}, \mathbf{d}_h^n, \dot{\mathbf{d}}_h^n)\}_{n \geq 1} \subset \mathbf{V}_h \times Q_h \times \boldsymbol{\Lambda}_h \times \mathbf{W}_h \times \mathbf{W}_h \times \mathbf{W}_h$ be given by Algorithm 3.

- Scheme with $r = 1$. For $n \geq 1$, we have

$$(25) \quad E_h^n + D_h^n + \tau^2 \|\dot{\mathbf{d}}_h^n\|_s^2 + \frac{\tau}{2\rho^s \varepsilon} \|\mathbf{L}_h \mathbf{d}_h^n\|_{0,\Sigma}^2 \leq E_h^0 + \tau^2 \|\mathbf{d}_{1,h}\|_s^2 + \frac{\tau}{2\rho^s \varepsilon} \|\mathbf{L}_h \mathbf{d}_{0,h}\|_{0,\Sigma}^2.$$

- Scheme with $r = 2$. Let τ and h_s be such that there exist $\alpha > 0$ such that

$$(26) \quad \begin{cases} \tau \leq \alpha \left(\frac{\rho^s \varepsilon}{C_1} \right)^{\frac{2}{3}} h_s^{\frac{4}{3}}, \\ 2\tau\alpha^3 < 1, \end{cases}$$

then, for $n \geq 1$, we have

$$(27) \quad E_h^n + D_h^n \leq \exp\left(\frac{2\gamma t_n}{1-2\tau\gamma}\right) E_h^0.$$

Proof. By taking $\mathbf{v} = \mathbf{u}_h^n$, $q = p_h^n$, $\mathbf{w} = \dot{\mathbf{d}}_h^{n-\frac{1}{2}}$ and $\boldsymbol{\mu} = -\boldsymbol{\lambda}_h^n$ in (17), and using the well known equality $2(a-b, a) = (a^2 - b^2 + (a-b)^2)$, we have

$$(28) \quad \begin{aligned} & \frac{\rho^f}{2} (\|\mathbf{u}_h^n\|_{0,\Omega}^2 - \|\mathbf{u}_h^{n-1}\|_{0,\Omega}^2 + \|\mathbf{u}_h^n - \mathbf{u}_h^{n-1}\|_{0,\Omega}^2) + 2\tau\mu \|\boldsymbol{\epsilon}(\mathbf{u}_h^n)\|_{0,\Omega}^2 + \tau |p_h^n|_{s_h}^2 \\ & + \rho^s \varepsilon (\dot{\mathbf{d}}_h^{n-\frac{1}{2}} - \dot{\mathbf{d}}_h^{n-1}, \dot{\mathbf{d}}_h^{n-\frac{1}{2}})_{\Sigma} = -\tau a^s (\mathbf{d}_h^{n*}, \dot{\mathbf{d}}_h^{n-\frac{1}{2}}). \end{aligned}$$

On the other hand, by testing (23) with $\mathbf{w} = \dot{\mathbf{d}}_h^{n-\frac{1}{2}}$ and by adding the resulting equation to (28), we get

$$\begin{aligned} & \frac{\rho^f}{2} (\|\mathbf{u}_h^n\|_{0,\Omega}^2 - \|\mathbf{u}_h^{n-1}\|_{0,\Omega}^2 + \|\mathbf{u}_h^n - \mathbf{u}_h^{n-1}\|_{0,\Omega}^2) + 2\tau\mu \|\boldsymbol{\epsilon}(\mathbf{u}_h^n)\|_{0,\Omega}^2 + \tau |p_h^n|_{s_h}^2 \\ & + \rho^s \varepsilon (\dot{\mathbf{d}}_h^n - \dot{\mathbf{d}}_h^{n-1}, \dot{\mathbf{d}}_h^{n-\frac{1}{2}})_{\Sigma} + \tau a^s (\mathbf{d}_h^n, \dot{\mathbf{d}}_h^{n-\frac{1}{2}}) = 0. \end{aligned}$$

By introducing in the above equation the characterization of $\dot{\mathbf{d}}_h^{n-\frac{1}{2}}$ given in (22) yields

$$(29) \quad \begin{aligned} & \frac{\rho^f}{2} (\|\mathbf{u}_h^n\|_{0,\Omega}^2 - \|\mathbf{u}_h^{n-1}\|_{0,\Omega}^2 + \|\mathbf{u}_h^n - \mathbf{u}_h^{n-1}\|_{0,\Omega}^2) + 2\tau\mu \|\boldsymbol{\epsilon}(\mathbf{u}_h^n)\|_{0,\Omega}^2 + \tau |p_h^n|_{s_h}^2 \\ & + \frac{\rho^s \varepsilon}{2} (\|\dot{\mathbf{d}}_h^n\|_{0,\Sigma}^2 - \|\dot{\mathbf{d}}_h^{n-1}\|_{0,\Sigma}^2 + \|\dot{\mathbf{d}}_h^n - \dot{\mathbf{d}}_h^{n-1}\|_{0,\Sigma}^2) \\ & + \frac{1}{2} (\|\mathbf{d}_h^n\|_s^2 - \|\mathbf{d}_h^{n-1}\|_s^2 + \|\mathbf{d}_h^n - \mathbf{d}_h^{n-1}\|_s^2) + T_1 + T_2 = 0, \end{aligned}$$

with

$$T_1 := \tau (\dot{\mathbf{d}}_h^n - \dot{\mathbf{d}}_h^{n-1}, \mathbf{L}_h(\mathbf{d}_h^n - \mathbf{d}_h^{n*}))_{\Sigma} \quad T_2 := \frac{\tau^2}{\rho^s \varepsilon} a^s(\mathbf{d}_h^n, \mathbf{L}_h(\mathbf{d}_h^n - \mathbf{d}_h^{n*})).$$

We estimate this terms as in [29, Theorem 1], by treating each case of extrapolation separately.

Case $r = 1$. We have $\mathbf{d}_h^{n*} = \mathbf{d}_h^{n-1}$, so that $\mathbf{L}_h(\mathbf{d}_h^n - \mathbf{d}_h^{n*}) = \mathbf{L}_h(\mathbf{d}_h^n - \mathbf{d}_h^{n-1}) = \tau \mathbf{L}_h \dot{\mathbf{d}}_h^n$. By using the definition of the discrete operator \mathbf{L}_h we get the following relations for T_1 and T_2 :

$$\begin{aligned} T_1 &= \tau^2 \left(\dot{\mathbf{d}}_h^n - \dot{\mathbf{d}}_h^{n-1}, \mathbf{L}_h \dot{\mathbf{d}}_h^n \right)_\Sigma = \tau^2 a^s \left(\dot{\mathbf{d}}_h^n - \dot{\mathbf{d}}_h^{n-1}, \dot{\mathbf{d}}_h^n \right)_\Sigma \\ &= \frac{\tau}{2} \left(\|\dot{\mathbf{d}}_h^n\|_s^2 - \|\dot{\mathbf{d}}_h^{n-1}\|_s^2 + \|\dot{\mathbf{d}}_h^n - \dot{\mathbf{d}}_h^{n-1}\|_s^2 \right), \\ T_2 &= \frac{\tau^2}{\rho^s \varepsilon} \left(\mathbf{L}_h \mathbf{d}_h^n, \mathbf{L}_h(\mathbf{d}_h^n - \mathbf{d}_h^{n*}) \right)_\Sigma \\ &= \frac{\tau^2}{\rho^s \varepsilon} \left(\|\mathbf{L}_h \mathbf{d}_h^n\|_{0,\Sigma}^2 - \|\mathbf{L}_h \mathbf{d}_h^{n-1}\|_{0,\Sigma}^2 + \|\mathbf{L}_h(\mathbf{d}_h^n - \mathbf{d}_h^{n-1})\|_{0,\Sigma}^2 \right). \end{aligned}$$

By inserting these equalities into (29) and summing over n , we obtain (25).

Case $r = 2$. We have $\mathbf{d}_h^{n*} = \mathbf{d}_h^{n-1} + \tau \dot{\mathbf{d}}_h^{n-1}$, which yields

$$\mathbf{L}_h(\mathbf{d}_h^n - \mathbf{d}_h^{n*}) = \mathbf{L}_h(\mathbf{d}_h^n - \mathbf{d}_h^{n-1} - \tau \dot{\mathbf{d}}_h^{n-1}) = \tau \mathbf{L}_h(\dot{\mathbf{d}}_h^n - \dot{\mathbf{d}}_h^{n-1}).$$

Substituting the last relation in T_1 and T_2 gives

$$\begin{aligned} T_1 &= \tau^2 \left(\dot{\mathbf{d}}_h^n - \dot{\mathbf{d}}_h^{n-1}, \mathbf{L}_h(\dot{\mathbf{d}}_h^n - \dot{\mathbf{d}}_h^{n-1}) \right)_\Sigma \\ &= \tau^2 a^s (\dot{\mathbf{d}}_h^n - \dot{\mathbf{d}}_h^{n-1}, \dot{\mathbf{d}}_h^n - \dot{\mathbf{d}}_h^{n-1}) = \tau^2 \|\dot{\mathbf{d}}_h^n - \dot{\mathbf{d}}_h^{n-1}\|_s^2, \\ T_2 &= \frac{\tau^3}{\rho^s \varepsilon} a^s (\mathbf{d}_h^n, \mathbf{L}_h(\dot{\mathbf{d}}_h^n - \dot{\mathbf{d}}_h^{n-1})) = \frac{\tau^3}{\rho^s \varepsilon} a^s (\mathbf{L}_h \mathbf{d}_h^n, \dot{\mathbf{d}}_h^n - \dot{\mathbf{d}}_h^{n-1}) \\ &\geq -\frac{\tau^3}{\rho^s \varepsilon} \|\mathbf{L}_h \mathbf{d}_h^n\|_s \|\dot{\mathbf{d}}_h^n - \dot{\mathbf{d}}_h^{n-1}\|_s \\ &\geq -\frac{\tau^4 C_1^2}{(\rho^s \varepsilon)^2 h_s^4} \|\mathbf{d}_h^n\|_s^2 - \tau^2 \|\dot{\mathbf{d}}_h^n - \dot{\mathbf{d}}_h^{n-1}\|_s^2 \\ &\geq -\tau \alpha^3 \|\mathbf{d}_h^n\|_s^2 - \tau^2 \|\dot{\mathbf{d}}_h^n - \dot{\mathbf{d}}_h^{n-1}\|_s^2. \end{aligned}$$

In the two last bounds of T_2 , the inverse estimate (21), the Young's inequality and (26)₁ were used. By inserting these expression into (29) and by summing over n , we get

$$\begin{aligned} &\frac{\rho^f}{2} \|\mathbf{u}_h^n\|_{0,\Omega}^2 + \frac{\rho^s \varepsilon}{2} \|\dot{\mathbf{d}}_h^n\|_{0,\Sigma}^2 + \frac{1}{2} \|\mathbf{d}_h^n\|_s^2 + \tau \sum_{m=1}^n (2\mu \|\boldsymbol{\epsilon}(\mathbf{u}_h^m)\|_{0,\Omega}^2 + |p_h^m|_{s_h}^2) \\ &\leq \frac{\rho^f}{2} \|\mathbf{u}_{0,h}\|_{0,\Omega}^2 + \frac{\rho^s \varepsilon}{2} \|\mathbf{d}_{1,h}\|_{0,\Sigma}^2 + \frac{1}{2} \|\mathbf{d}_{0,h}\|_s^2 + \tau \sum_{m=1}^n \alpha^3 \|\mathbf{d}_h^m\|_s^2. \end{aligned}$$

Finally, the estimate (27) follows by applying the discrete Gronwall's Lemma 1 with $\gamma_m := 2\alpha^3$ and by assuming that (26)₂ holds. \square

4.2. Error estimates for a linear model problem. This section is devoted to the convergence analysis of Algorithm 3 by assuming that the structure undergoes infinitesimal displacements. We can hence identify the current configuration with the reference one. Therefore the terms in Problem 2 and in Algorithm 3 which contain the composition of a function v with the mappings ϕ and ϕ_h^{n-1} , respectively, will be written simply as $v|_\Sigma$ instead of $v \circ \phi$. Moreover, in order to simplify the presentation, we drop out the non-linear convective term in the fluid and we assume

that the immersed structure is represented by a closed polygonal line or surface (see Fig. 1). As a consequence the discrete spaces \mathbf{W}_h and $\mathbf{\Lambda}_h$ coincide,

$$(30) \quad \mathbf{W}_h = \mathbf{\Lambda}_h.$$

Since the pressure results to be discontinuous across the structure, we assume that the solution enjoys the following regularity properties for $0 < \ell < 1/2$ and $0 < m \leq 1$:

$$(31) \quad \begin{aligned} \mathbf{u} &\in (H^1(0, T; H^{1+\ell}(\Omega)))^d, & \partial_{tt}\mathbf{u} &\in (L^2(0, T; L^2(\Omega)))^d, \\ p &\in H^1(0, T; H^\ell(\Omega)), & \boldsymbol{\lambda} &\in H^1(0, T; H^{\ell-1/2}(\Sigma))^d, \\ \mathbf{d} &\in (H^1(0, T; H^{1+m}(\Sigma)))^d, & \mathbf{Ld} &\in (L^\infty(0, T; L^2(\Sigma)))^d, \\ \dot{\mathbf{d}} &\in (H^1(0, T; H^{1+m}(\Sigma)))^d, & \partial_{tt}\dot{\mathbf{d}} &\in (L^2(0, T; L^2(\Sigma)))^d. \end{aligned}$$

We introduce the projection operators which will be used in the proof of the error estimates together with some approximation results. Let $\mathbf{\Pi}_V : H_0^1(\Omega)^d \times L_0^2(\Omega) \rightarrow \mathbf{V}_h$ and $\mathbf{\Pi}_Q : H_0^1(\Omega)^d \times L_0^2(\Omega) \rightarrow Q_h$ be the *Stokes projection* operators which to any pair $(\mathbf{u}, p) \in H_0^1(\Omega)^d \times L_0^2(\Omega)$ associate the solution $(\mathbf{\Pi}_V(\mathbf{u}, p), \mathbf{\Pi}_Q(\mathbf{u}, p)) \in \mathbf{V}_h \times Q_h$ of the following discrete Stokes equations

$$(32) \quad a_h^f((\mathbf{\Pi}_V(\mathbf{u}, p), \mathbf{\Pi}_Q(\mathbf{u}, p)), (\mathbf{v}, q)) = a^f((\mathbf{u}, p), (\mathbf{v}, q)) \quad \forall (\mathbf{v}, q) \in \mathbf{V}_h \times Q_h.$$

Exploiting carefully the stabilization term appearing in the Stokes equations discretized by the stabilized $\mathbb{P}_1/\mathbb{P}_1$ elements, one can extend the standard error estimates to the case of non smooth pressure and velocity, as follows:

$$(33) \quad \|\mathbf{u} - \mathbf{\Pi}_V(\mathbf{u}, p)\|_{1,\Omega} + \|p - \mathbf{\Pi}_Q(\mathbf{u}, p)\|_{0,\Omega} \leq Ch_f^\ell (\|\mathbf{u}\|_{1+\ell,\Omega} + \|p\|_{\ell,\Omega}).$$

Moreover, assuming that the domain Ω is convex, by standard duality argument one can obtain the estimate in the L^2 -norm for the velocity, namely

$$(34) \quad \|\mathbf{u} - \mathbf{\Pi}_V(\mathbf{u}, p)\|_{0,\Omega} \leq Ch_f^{1+\ell} (\|\mathbf{u}\|_{1+\ell,\Omega} + \|p\|_{\ell,\Omega}).$$

We denote by $\mathbf{\Pi}_W : \mathbf{W} \rightarrow \mathbf{W}_h$ the elliptic projection operator associated to the bilinear form a^s as follows: for any $\mathbf{d} \in \mathbf{W}$, $\mathbf{\Pi}_W \mathbf{d} \in \mathbf{W}_h$ with

$$(35) \quad a^s(\mathbf{\Pi}_W \mathbf{d}, \mathbf{w}_h) = a^s(\mathbf{d}, \mathbf{w}_h) \quad \forall \mathbf{w}_h \in \mathbf{W}_h.$$

Since a^s is assumed to be coercive on \mathbf{W} the following approximation estimate holds true

$$(36) \quad \|\mathbf{d} - \mathbf{\Pi}_W \mathbf{d}\|_s \leq Ch_s^m \|\mathbf{d}\|_{1+m,\Sigma}.$$

At the end, we introduce the projection operator $\mathbf{\Pi}_\Lambda : \mathbf{\Lambda} \rightarrow \mathbf{\Lambda}_h$ for the Lagrange multiplier as follows:

$$(37) \quad \mathbf{c}(\mathbf{\Pi}_\Lambda \boldsymbol{\lambda}, \mathbf{w}_h) = \mathbf{c}(\boldsymbol{\lambda}, \mathbf{w}_h) \quad \forall \mathbf{w}_h \in \mathbf{W}_h.$$

We observe that we have used the same discrete space for $\mathbf{\Lambda}_h$ and \mathbf{W}_h and that for smooth functions the bilinear form \mathbf{c} can be seen as the scalar product in $L^2(\Sigma)$. Then we have the following approximation property.

Lemma 4. *Assume that \mathcal{S}_h be quasi-uniform. We have*

$$(38) \quad \|\boldsymbol{\lambda} - \mathbf{\Pi}_\Lambda \boldsymbol{\lambda}\|_\Lambda \leq Ch_s^\ell \|\boldsymbol{\lambda}\|_{\ell-\frac{1}{2},\Sigma}$$

for any $\boldsymbol{\lambda} \in H^{\ell-\frac{1}{2}}(\Sigma)^d$.

Proof. In the following we shall use the L^2 -projection P_0 onto \mathbf{W}_h defined by

$$(\mathbf{w} - P_0 \mathbf{w}, \mathbf{z})_\Sigma = 0 \quad \forall \mathbf{z} \in \mathbf{W}_h.$$

By definition of the norm in the space Λ and using (30), we have

$$\begin{aligned}
\|\boldsymbol{\lambda} - \Pi_\Lambda \boldsymbol{\lambda}\|_\Lambda &= \sup_{\mathbf{z} \in H^{\frac{1}{2}}(\Sigma)^d} \frac{\mathbf{c}(\boldsymbol{\lambda} - \Pi_\Lambda \boldsymbol{\lambda}, \mathbf{z})}{\|\mathbf{z}\|_{\frac{1}{2}, \Sigma}} \\
&= \sup_{\mathbf{z} \in H^{\frac{1}{2}}(\Sigma)^d} \frac{\mathbf{c}(\boldsymbol{\lambda} - \Pi_\Lambda \boldsymbol{\lambda}, \mathbf{z} - P_0 \mathbf{z})}{\|\mathbf{z}\|_{\frac{1}{2}, \Sigma}} \\
(39) \quad &= \sup_{\mathbf{z} \in H^{\frac{1}{2}}(\Sigma)^d} \frac{\mathbf{c}(\boldsymbol{\lambda}, \mathbf{z} - P_0 \mathbf{z}) - (\Pi_\Lambda \boldsymbol{\lambda}, \mathbf{z} - P_0 \mathbf{z})_\Sigma}{\|\mathbf{z}\|_{\frac{1}{2}, \Sigma}} \\
&= \sup_{\mathbf{w} \in H^{\frac{1}{2}}(\Sigma)^d} \frac{\mathbf{c}(\boldsymbol{\lambda}, \mathbf{w} - P_0 \mathbf{w})}{\|\mathbf{w}\|_{\frac{1}{2}, \Sigma}} \\
&\leq \sup_{\mathbf{w} \in H^{\frac{1}{2}}(\Sigma)^d} \frac{\|\boldsymbol{\lambda}\|_{\ell-\frac{1}{2}, \Sigma} \|\mathbf{w} - P_0 \mathbf{w}\|_{\frac{1}{2}-\ell, \Sigma}}{\|\mathbf{w}\|_{\frac{1}{2}, \Sigma}}.
\end{aligned}$$

It remains to bound $\|\mathbf{w} - P_0 \mathbf{w}\|_{H^{1/2-\ell}(\Sigma)^d}$. Since the mesh is quasi uniform, we observe that the L^2 -projection is stable in $H^1(\Sigma)$, see [5] and the references quoted therein which can weaken the requirement of a quasi-uniform mesh. Therefore by application of interpolation operator theory (see for example [20]) P_0 is stable also in $H^{1/2}(\Sigma)$, so that there exists a constant c_0 such that

$$\|P_0 \mathbf{w}\|_{\frac{1}{2}, \Sigma} \leq c_0 \|\mathbf{w}\|_{\frac{1}{2}, \Sigma}.$$

This implies the following error estimates

$$\begin{aligned}
\|\mathbf{w} - P_0 \mathbf{w}\|_{0, \Sigma} &\leq Ch^{\frac{1}{2}} \|\mathbf{w}\|_{\frac{1}{2}, \Sigma} \\
\|\mathbf{w} - P_0 \mathbf{w}\|_{\frac{1}{2}, \Sigma} &\leq (1 + c_0) \|\mathbf{w}\|_{\frac{1}{2}, \Sigma}.
\end{aligned}$$

Applying again the interpolation operator theory, we arrive at the desired estimate

$$\|\mathbf{w} - P_0 \mathbf{w}\|_{\frac{1}{2}-\ell, \Sigma} \leq Ch^\ell \|\mathbf{w}\|_{\frac{1}{2}, \Sigma}$$

and this inserted in (39) concludes the proof. \square

The following auxiliary result provides an estimate of the error between the time derivative and the backward finite difference approximation.

Lemma 5. *Let X be a real Hilbert space endowed with the norm $\|\cdot\|_X$. Then for all $\mathbf{v} \in H^2(0, T; X)$ we have*

$$(40) \quad \tau \|\partial_\tau \mathbf{v}^n - \partial_t \mathbf{v}^n\|_X \leq \tau^{\frac{3}{2}} \|\partial_{tt} \mathbf{v}\|_{L^2(t_{n-1}, t_n; X)}.$$

Moreover, for all $\mathbf{v} \in H^1(0, T; X)$ it holds true

$$(41) \quad \tau \|\partial_\tau \mathbf{v}^n\|_X \leq \tau^{\frac{1}{2}} \|\partial_t \mathbf{v}\|_{L^2(t_{n-1}, t_n; X)}.$$

We bound the three terms on the right hand side separately. An inverse inequality, trace theorem and the error estimates above imply

$$\mathbf{c}(\boldsymbol{\omega}_h^n, \bar{\mathbf{v}}|_\Sigma - \bar{\mathbf{v}}_h|_\Sigma) \leq C \left(\frac{h_f}{h_s} \right)^{\frac{1}{2}} \|\boldsymbol{\omega}_h^n\|_\Lambda \|\bar{\mathbf{v}}\|_{1,\Omega}.$$

For the second term we use Lemma 4 as follows

$$\mathbf{c}(\boldsymbol{\lambda}_\Pi^n - \boldsymbol{\lambda}^n, \bar{\mathbf{v}}_h|_\Sigma) \leq C \|\boldsymbol{\omega}_\Pi^n\|_\Lambda \|\bar{\mathbf{v}}\|_{1,\Omega}.$$

We use the first equation in (42), the definition of the Stokes projection operator (32) and (45) to estimate the last term in (47), namely

$$\begin{aligned} \mathbf{c}(\boldsymbol{\lambda}^n - \boldsymbol{\lambda}_h^n, \bar{\mathbf{v}}_h|_\Sigma) &= -\rho^f (\partial_t \mathbf{u}^n - \partial_\tau \mathbf{u}_h^n, \bar{\mathbf{v}}_h) - 2\mu(\boldsymbol{\epsilon}(\mathbf{u}^n - \mathbf{u}_h^n), \boldsymbol{\epsilon}(\bar{\mathbf{v}}_h)) \\ &\quad + (\operatorname{div} \bar{\mathbf{v}}_h, p^n - p_h^n) \\ &= -\rho^f ((\partial_t - \partial_\tau) \mathbf{u}^n, \bar{\mathbf{v}}_h) - \rho^f (\partial_\tau (\boldsymbol{\theta}_\Pi^n + \boldsymbol{\theta}_h^n), \bar{\mathbf{v}}_h) \\ &\quad - 2\mu(\boldsymbol{\epsilon}(\boldsymbol{\theta}_h^n), \boldsymbol{\epsilon}(\bar{\mathbf{v}}_h)) - s_h(\bar{p}_h, \phi_h^n) \\ &\leq C \|\bar{\mathbf{v}}\|_1 (\tau^{\frac{1}{2}} \|\partial_{tt} \mathbf{u}\|_{L^2(t_{n-1}, t_n; L^2(\Omega)^d)} \\ &\quad + \|\partial_\tau (\boldsymbol{\theta}_\Pi^n + \boldsymbol{\theta}_h^n)\|_{0,\Omega} + \|\boldsymbol{\epsilon}(\boldsymbol{\theta}_h^n)\|_{0,\Omega} + |\phi_h^n|_{s_h}). \end{aligned}$$

Putting together the last inequalities in (47) and taking into account (46), we obtain

$$\begin{aligned} \beta \|\boldsymbol{\omega}_h^n\|_\Lambda &\leq C \left(\frac{h_f}{h_s} \right)^{1/2} \|\boldsymbol{\omega}_h^n\|_\Lambda + C \left(\|\boldsymbol{\omega}_\Pi^n\|_\Lambda + \tau^{1/2} \|\partial_{tt} \mathbf{u}\|_{L^2(t_{n-1}, t_n; L^2(\Omega)^d)} \right. \\ &\quad \left. + \|\partial_\tau (\boldsymbol{\theta}_\Pi^n + \boldsymbol{\theta}_h^n)\|_{0,\Omega} + \|\boldsymbol{\epsilon}(\boldsymbol{\theta}_h^n)\|_{0,\Omega} + |\phi_h^n|_{s_h} \right). \end{aligned}$$

Choosing h_f/h_s sufficiently small we get (44), which concludes the proof. \square

The solid intermediate velocity $\dot{\mathbf{d}}_h^{n-\frac{1}{2}}$ provided in Step 1 of Algorithm 3 is actually an approximation of $\dot{\mathbf{d}}_h^n$, hence we introduce the following error

$$\boldsymbol{\chi}_h^n = \dot{\mathbf{d}}_\Pi^n - \dot{\mathbf{d}}_h^{n-\frac{1}{2}}.$$

Hence, owing to (22), we have

$$(48) \quad \boldsymbol{\chi}_h^n = \dot{\boldsymbol{\xi}}_h^n - \frac{\tau}{\rho^s \varepsilon} \mathbf{L}_h(\mathbf{d}_h^n - \mathbf{d}_h^{n*}) = \dot{\boldsymbol{\xi}}_h^n + \frac{\tau}{\rho^s \varepsilon} \mathbf{L}_h(\boldsymbol{\xi}_h^n - \boldsymbol{\xi}_h^{n*}) - \frac{\tau}{\rho^s \varepsilon} \mathbf{L}_h(\mathbf{d}^n - \mathbf{d}^{n*}).$$

The following theorem states the main result of this section. It provides an error bound on the discrete approximation errors.

Theorem 2. *Let $(\mathbf{u}^n, p^n, \mathbf{d}^n, \dot{\mathbf{d}}^n, \boldsymbol{\lambda}^n) \in H_0^1(\Omega)^d \times L_0^2(\Omega) \times \mathbf{W} \times \mathbf{W} \times \Lambda$ be the solution of Problem 2 and let $(\mathbf{u}_h^n, p_h^n, \dot{\mathbf{d}}_h^{n-\frac{1}{2}}, \boldsymbol{\lambda}^n) \in \mathbf{V}_h \times Q_h \times \mathbf{W}_h \times \Lambda_h$ and $(\mathbf{d}_h^n, \dot{\mathbf{d}}_h^n) \in \mathbf{W}_h \times \mathbf{W}_h$ be given by Algorithm 3, respectively. Then, if h_f/h_s is sufficiently small, the following bounds hold true:*

- Scheme with $r = 1$:

$$\begin{aligned}
(49) \quad & \rho^f \|\boldsymbol{\theta}_h^n\|_{0,\Omega}^2 + \rho^s \varepsilon \|\dot{\boldsymbol{\xi}}_h^n\|_{0,\Sigma}^2 + \|\boldsymbol{\xi}_h^n\|_s^2 \\
& \leq C \left(\tau^2 \|\partial_{tt} \mathbf{u}\|_{L^2(0,t_n;L^2(\Omega)^d)}^2 + \tau^2 \|\partial_{tt} \dot{\mathbf{d}}\|_{L^2(0,t_n;L^2(\Sigma)^d)}^2 \right. \\
& \quad + \tau^2 \|\partial_{tt} \mathbf{d}\|_{L^2(0,t_n;H^1(\Sigma)^d)}^2 + \tau^5 \|\partial_{tt} \dot{\mathbf{d}}\|_{L^2(0,t_n;H^1(\Sigma)^d)}^2 + \|\partial_t \boldsymbol{\theta}_\Pi\|_{L^2(0,t_n;L^2(\Omega)^d)}^2 \\
& \quad + \|\partial_t \dot{\boldsymbol{\xi}}_\Pi\|_{L^2(0,t_n;L^2(\Sigma)^d)}^2 + \tau \|\partial_t \boldsymbol{\xi}_\Pi\|_{L^2(0,t_n;L^2(H^1(\Sigma)^d))}^2 \\
& \quad + \tau^3 \|\partial_\tau \dot{\boldsymbol{\xi}}_\Pi\|_{L^2(0,t_n;L^2(H^1(\Sigma)^d))}^2 + \tau^2 \|\partial_t \mathbf{Ld}\|_{L^2(0,t_n;L^2(\Sigma)^d)}^2 \\
& \quad \left. + \sum_{k=1}^n (\tau \|\boldsymbol{\omega}_\Pi^k\|_\Lambda^2 + \tau \|\boldsymbol{\theta}_\Pi^k\|_{1,\Omega}^2 + \tau \|\dot{\boldsymbol{\xi}}_\Pi^k\|_{\frac{1}{2},\Sigma}^2 + \tau^2 \|\dot{\boldsymbol{\xi}}_\Pi^k\|_s^2) \right).
\end{aligned}$$

- Scheme with $r = 2$: let τ such that (26) holds true and

$$\frac{\tau^3}{(\rho^s \varepsilon)^2} \leq 1$$

then for $n \geq 1$

$$\begin{aligned}
(50) \quad & \rho^f \|\boldsymbol{\theta}_h^n\|_{0,\Omega}^2 + \rho^s \varepsilon \|\dot{\boldsymbol{\xi}}_h^n\|_{0,\Sigma}^2 + \|\boldsymbol{\xi}_h^n\|_s^2 \\
& \leq C \left(\tau^2 \|\partial_{tt} \mathbf{u}\|_{L^2(0,t_n;L^2(\Omega)^d)}^2 + \tau^2 \|\partial_{tt} \dot{\mathbf{d}}\|_{L^2(0,t_n;L^2(\Sigma)^d)}^2 \right. \\
& \quad + \tau^2 \|\partial_{tt} \mathbf{d}\|_{L^2(0,t_n;H^1(\Sigma)^d)}^2 + \|\partial_t \boldsymbol{\theta}_\Pi\|_{L^2(0,t_n;L^2(\Omega)^d)}^2 + \|\partial_t \dot{\boldsymbol{\xi}}_\Pi\|_{L^2(0,t_n;L^2(\Sigma)^d)}^2 \\
& \quad + \tau^3 \|\partial_t \dot{\boldsymbol{\xi}}_\Pi\|_{L^2(0,t_n;H^1(\Sigma)^d)}^2 + \tau^5 \|\partial_t \mathbf{Ld}\|_{L^2(0,t_n;L^2(\Sigma)^d)}^2 \\
& \quad \left. + \sum_{k=1}^n (\tau \|\boldsymbol{\omega}_\Pi^k\|_\Lambda^2 + \tau \|\boldsymbol{\theta}_\Pi^k\|_{1,\Omega}^2 + \tau \|\dot{\boldsymbol{\xi}}_\Pi^k\|_{\frac{1}{2},\Sigma}^2) \right).
\end{aligned}$$

Proof. By using the notation introduced in (43) and recalling the definitions of the projection operators introduced in (32), (35) and (37), the error equation (42) yields

$$(51) \quad \begin{cases} \rho^f (\partial_\tau \boldsymbol{\theta}_h^n, \mathbf{v}) + 2\mu (\boldsymbol{\epsilon}(\boldsymbol{\theta}_h^n), \boldsymbol{\epsilon}(\mathbf{v})) - (\operatorname{div} \mathbf{v}, \phi_h^n) + \mathbf{c}(\boldsymbol{\omega}_h^n, \mathbf{v}|_\Sigma) \\ \quad = -\rho^f (\partial_t \mathbf{u}^n - \partial_\tau \mathbf{u}^n, \mathbf{v}) - \rho^f (\partial_\tau \boldsymbol{\theta}_\Pi^n, \mathbf{v}) - \mathbf{c}(\boldsymbol{\omega}_\Pi^n, \mathbf{v}|_\Sigma) & \forall \mathbf{v} \in \mathbf{V}_h, \\ (\operatorname{div}(\boldsymbol{\theta}_h^n, q) + s_h(\phi_h^n, q) = 0 & \forall q \in Q_h, \\ \mathbf{c}(\boldsymbol{\mu}, \boldsymbol{\theta}_h^n|_\Sigma - \boldsymbol{\chi}_h^n) = -\mathbf{c}(\boldsymbol{\mu}, \boldsymbol{\theta}_\Pi^n|_\Sigma - \dot{\boldsymbol{\xi}}_\Pi^n) & \forall \boldsymbol{\mu} \in \boldsymbol{\Lambda}_h, \\ \rho^s \varepsilon (\partial_\tau \dot{\boldsymbol{\xi}}_h^n, \mathbf{w})_\Sigma + a^s(\boldsymbol{\xi}_h^n, \mathbf{w}) - \mathbf{c}(\boldsymbol{\omega}_h^n, \mathbf{w}) \\ \quad = -\rho^s \varepsilon (\partial_t \dot{\mathbf{d}}^n - \partial_\tau \dot{\mathbf{d}}^n, \mathbf{w})_\Sigma - \rho^s \varepsilon (\partial_\tau \dot{\boldsymbol{\xi}}_\Pi^n, \mathbf{w})_\Sigma & \forall \mathbf{w} \in \mathbf{W}_h, \\ \partial_\tau \boldsymbol{\xi}_h^n = \dot{\boldsymbol{\xi}}_h^n - \dot{\mathbf{d}}_\Pi^n + \partial_\tau \mathbf{d}_\Pi^n. \end{cases}$$

We take $\mathbf{v} = \tau \boldsymbol{\theta}_h^n$, $q = \tau \phi_h^n$, $\mathbf{w} = \tau \boldsymbol{\chi}_h^n$, $\boldsymbol{\mu} = -\tau \boldsymbol{\omega}_h^n$ and sum the resulting expressions, so that we have

$$\begin{aligned}
& \rho^f (\boldsymbol{\theta}_h^n - \boldsymbol{\theta}_h^{n-1}, \boldsymbol{\theta}_h^n) + \tau 2\mu (\boldsymbol{\epsilon}(\boldsymbol{\theta}_h^n), \boldsymbol{\epsilon}(\boldsymbol{\theta}_h^n)) + \tau s_h(\phi_h^n, \phi_h^n) \\
& \quad + \rho^s \varepsilon (\dot{\boldsymbol{\xi}}_h^n - \dot{\boldsymbol{\xi}}_h^{n-1}, \boldsymbol{\chi}_h^n)_\Sigma + \tau a^s(\boldsymbol{\xi}_h^n, \boldsymbol{\chi}_h^n) \\
& = -\tau \rho^f (\partial_t \mathbf{u}^n - \partial_\tau \mathbf{u}^n, \boldsymbol{\theta}_h^n) - \tau \rho^f (\partial_\tau \boldsymbol{\theta}_\Pi^n, \boldsymbol{\theta}_h^n) - \tau \mathbf{c}(\boldsymbol{\omega}_\Pi^n, \boldsymbol{\theta}_h^n|_\Sigma) \\
& \quad - \tau \rho^s \varepsilon (\partial_t \dot{\mathbf{d}}^n - \partial_\tau \dot{\mathbf{d}}^n, \boldsymbol{\chi}_h^n)_\Sigma - \tau \rho^s \varepsilon (\partial_\tau \dot{\boldsymbol{\xi}}_\Pi^n, \boldsymbol{\chi}_h^n)_\Sigma + \tau \mathbf{c}(\boldsymbol{\omega}_h^n, \boldsymbol{\theta}_\Pi^n|_\Sigma - \dot{\boldsymbol{\xi}}_\Pi^n).
\end{aligned}$$

We observe that using (48), last equation in (51) and (35), we have

$$a^s(\boldsymbol{\xi}_h^n, \boldsymbol{\chi}_h^n) = a^s(\boldsymbol{\xi}_h^n, \partial_\tau \boldsymbol{\xi}_h^n) + a^s(\boldsymbol{\xi}_h^n, \partial_t \mathbf{d}^n - \partial_\tau \mathbf{d}^n).$$

Using the well-known identity $(a-b)a = \frac{1}{2}(a^2 - b^2 + (a-b)^2)$ and (48), we get

$$(52) \quad \begin{aligned} & \frac{\rho^f}{2} (\|\boldsymbol{\theta}_h^n\|_{0,\Omega}^2 - \|\boldsymbol{\theta}_h^{n-1}\|_{0,\Omega}^2 + \|\boldsymbol{\theta}_h^n - \boldsymbol{\theta}_h^{n-1}\|_{0,\Omega}^2) + 2\tau\mu \|\boldsymbol{\epsilon}(\boldsymbol{\theta}_h^n)\|_{0,\Omega}^2 + \tau|\phi_h^n|_{s_h} \\ & + \frac{\rho^s \varepsilon}{2} (\|\dot{\boldsymbol{\xi}}_h^n\|_{0,\Sigma}^2 - \|\dot{\boldsymbol{\xi}}_h^{n-1}\|_{0,\Sigma}^2 + \|\dot{\boldsymbol{\xi}}_h^n - \dot{\boldsymbol{\xi}}_h^{n-1}\|_{0,\Sigma}^2) \\ & + \frac{1}{2} (\|\boldsymbol{\xi}_h^n\|_s^2 - \|\boldsymbol{\xi}_h^{n-1}\|_s^2 + \|\boldsymbol{\xi}_h^n - \boldsymbol{\xi}_h^{n-1}\|_s^2) = \sum_{i=1}^8 T_i, \end{aligned}$$

with the notations

$$(53) \quad \begin{aligned} T_1 &:= -\tau\rho^f(\partial_t \mathbf{u}^n - \partial_\tau \mathbf{u}^n, \boldsymbol{\theta}_h^n) - \tau\rho^f(\partial_\tau \boldsymbol{\theta}_\Pi^n, \boldsymbol{\theta}_h^n), \\ T_2 &:= -\tau\rho^s \varepsilon (\partial_t \dot{\mathbf{d}}^n - \partial_\tau \dot{\mathbf{d}}^n, \dot{\boldsymbol{\xi}}_h^n)_\Sigma - \tau\rho^s \varepsilon (\partial_\tau \dot{\boldsymbol{\xi}}_\Pi^n, \dot{\boldsymbol{\xi}}_h^n)_\Sigma, \\ T_3 &:= -\tau a^s(\boldsymbol{\xi}_h^n, \partial_t \mathbf{d}^n - \partial_\tau \mathbf{d}^n), \\ T_4 &:= -\tau \mathbf{c}(\boldsymbol{\omega}_\Pi^n, \boldsymbol{\theta}_h^n|_\Sigma), \\ T_5 &:= \tau \mathbf{c}(\boldsymbol{\omega}_h^n, \boldsymbol{\theta}_\Pi^n|_\Sigma - \dot{\boldsymbol{\xi}}_\Pi^n), \\ T_6 &:= \frac{\tau^2}{\rho^s \varepsilon} a^s(\boldsymbol{\xi}_h^n, \mathbf{L}_h(\mathbf{d}_h^n - \mathbf{d}_h^{n*})), \\ T_7 &:= \tau(\dot{\boldsymbol{\xi}}_h^n - \dot{\boldsymbol{\xi}}_h^{n-1}, \mathbf{L}_h(\mathbf{d}_h^n - \mathbf{d}_h^{n*}))_\Sigma, \\ T_8 &:= \tau^2(\partial_t \dot{\mathbf{d}}^n - \partial_\tau \dot{\mathbf{d}}^n, \mathbf{L}_h(\mathbf{d}_h^n - \mathbf{d}_h^{n*}))_\Sigma + \tau^2(\partial_\tau \dot{\boldsymbol{\xi}}_\Pi^n, \mathbf{L}_h(\mathbf{d}_h^n - \mathbf{d}_h^{n*}))_\Sigma. \end{aligned}$$

We estimate the first 5 terms which do not depend on \mathbf{d}_h^{n*} using Lemmas 5 and 6, which yields

$$(54) \quad \begin{aligned} T_1 &\leq C\rho^f \left(\tau^{3/2} \|\partial_{tt} \mathbf{u}\|_{L^2(t_{n-1}, t_n; L^2(\Omega)^d)} + \tau^{1/2} \|\partial_t \boldsymbol{\theta}_\Pi^n\|_{L^2(t_{n-1}, t_n; L^2(\Omega)^d)} \right) \|\boldsymbol{\theta}_h^n\|_{0,\Omega}, \\ T_2 &\leq C\rho^s \varepsilon \left(\tau^{3/2} \|\partial_{tt} \dot{\mathbf{d}}\|_{L^2(t_{n-1}, t_n; L^2(\Sigma)^d)} + \tau^{1/2} \|\partial_t \dot{\boldsymbol{\xi}}_\Pi^n\|_{L^2(t_{n-1}, t_n; L^2(\Sigma)^d)} \right) \|\dot{\boldsymbol{\xi}}_h^n\|_{0,\Sigma}, \\ T_3 &\leq C\tau^{3/2} \|\partial_{tt} \mathbf{d}\|_{L^2(t_{n-1}, t_n; H^1(\Sigma)^d)} \|\boldsymbol{\xi}_h^n\|_s, \\ T_4 &\leq C\tau \|\boldsymbol{\omega}_\Pi^n\|_\Lambda \|\boldsymbol{\theta}_h^n\|_{1,\Omega}, \\ T_5 &\leq C\tau \|\boldsymbol{\omega}_h^n\|_\Lambda \left(\|\boldsymbol{\theta}_\Pi^n\|_{1,\Omega} + \|\dot{\boldsymbol{\xi}}_\Pi^n\|_{\frac{1}{2},\Sigma} \right). \end{aligned}$$

Using Young's inequality in (54) and the Korn inequality $K\|\mathbf{v}\|_{1,\Omega} \leq \|\boldsymbol{\epsilon}(\mathbf{v})\|_{0,\Omega}$ for all $\mathbf{v} \in H_0^1(\Omega)^d$, and adding the resulting inequalities to (52) we have

$$\begin{aligned}
& \frac{\rho^f}{2} (\|\boldsymbol{\theta}_h^n\|_{0,\Omega}^2 - \|\boldsymbol{\theta}_h^{n-1}\|_{0,\Omega}^2 + \|\boldsymbol{\theta}_h^n - \boldsymbol{\theta}_h^{n-1}\|_{0,\Omega}^2) + 2\tau\mu K^2 \|\boldsymbol{\theta}_h^n\|_{1,\Omega}^2 + \tau|\phi_h^n|_{s_h} \\
& + \frac{\rho^s \varepsilon}{2} (\|\dot{\boldsymbol{\xi}}_h^n\|_{0,\Sigma}^2 - \|\dot{\boldsymbol{\xi}}_h^{n-1}\|_{0,\Sigma}^2 + \|\dot{\boldsymbol{\xi}}_h^n - \dot{\boldsymbol{\xi}}_h^{n-1}\|_{0,\Sigma}^2) \\
& + \frac{1}{2} (\|\boldsymbol{\xi}_h^n\|_s^2 - \|\boldsymbol{\xi}_h^{n-1}\|_s^2 + \|\boldsymbol{\xi}_h^n - \boldsymbol{\xi}_h^{n-1}\|_s^2) \\
(55) \quad & \leq \frac{\tau\delta_1}{2} \left(\rho^f \|\boldsymbol{\theta}_h^n\|_{0,\Omega}^2 + \rho^s \varepsilon \|\dot{\boldsymbol{\xi}}_h^n\|_{0,\Sigma}^2 + \|\boldsymbol{\xi}_h^n\|_s^2 + \|\boldsymbol{\theta}_h^n\|_{1,\Omega}^2 + |\phi_h^n|_{s_h}^2 \right) \\
& + C \left(\tau^2 \|\partial_{tt} \mathbf{u}\|_{L^2(t_{n-1}, t_n; L^2(\Omega)^d)}^2 + \tau^2 \|\partial_{tt} \mathbf{d}\|_{L^2(t_{n-1}, t_n; L^2(\Sigma)^d)}^2 \right) \\
& + \tau^2 \|\partial_{tt} \mathbf{d}\|_{L^2(t_{n-1}, t_n; H^1(\Sigma)^d)}^2 + \|\partial_t \boldsymbol{\theta}_\Pi^n\|_{L^2(t_{n-1}, t_n; L^2(\Omega)^d)}^2 \\
& + \|\partial_t \dot{\boldsymbol{\xi}}_\Pi^n\|_{L^2(t_{n-1}, t_n; L^2(\Sigma)^d)}^2 + \tau \|\boldsymbol{\omega}_\Pi^n\|_\Lambda^2 + \tau \|\boldsymbol{\theta}_\Pi^n\|_{1,\Omega}^2 + \tau \|\dot{\boldsymbol{\xi}}_\Pi^n\|_{\frac{1}{2},\Sigma}^2 \Big) + \sum_{i=6}^8 T_i.
\end{aligned}$$

For the remaining three terms T_i for $i = 6, 7, 8$ we have to take into account the definition of \mathbf{d}_h^{n*} .

Case $r = 1$. We estimate the term T_6 by noting that $\mathbf{d}_h^n = \mathbf{d}_\Pi^n - \boldsymbol{\xi}_h^n$ and using (19). We have,

$$\begin{aligned}
T_6 &= \frac{\tau^2}{\rho^s \varepsilon} a^s(\boldsymbol{\xi}_h^n, \mathbf{L}_h(\mathbf{d}_h^n - \mathbf{d}_h^{n-1})) \\
&= -\frac{\tau^2}{\rho^s \varepsilon} a^s(\boldsymbol{\xi}_h^n, \mathbf{L}_h(\boldsymbol{\xi}_h^n - \boldsymbol{\xi}_h^{n-1})) + \frac{\tau^2}{\rho^s \varepsilon} a^s(\boldsymbol{\xi}_h^n, \mathbf{L}_h(\mathbf{d}_\Pi^n - \mathbf{d}_\Pi^{n-1})) \\
(56) \quad &= -\frac{\tau^2}{\rho^s \varepsilon} (\mathbf{L}_h \boldsymbol{\xi}_h^n, \mathbf{L}_h(\boldsymbol{\xi}_h^n - \boldsymbol{\xi}_h^{n-1}))_\Sigma + \frac{\tau^2}{\rho^s \varepsilon} (\mathbf{L}_h \boldsymbol{\xi}_h^n, \mathbf{L}_h(\mathbf{d}_\Pi^n - \mathbf{d}_\Pi^{n-1}))_\Sigma \\
&\leq -\frac{1}{2} \frac{\tau^2}{\rho^s \varepsilon} (\|\mathbf{L}_h \boldsymbol{\xi}_h^n\|_{0,\Sigma}^2 - \|\mathbf{L}_h \boldsymbol{\xi}_h^{n-1}\|_{0,\Sigma}^2 + \|\mathbf{L}_h(\boldsymbol{\xi}_h^n - \boldsymbol{\xi}_h^{n-1})\|_{0,\Sigma}^2) \\
&\quad + \frac{\tau^2}{\rho^s \varepsilon} \|\mathbf{L}_h \boldsymbol{\xi}_h^n\|_{0,\Sigma} \|\mathbf{L}_h(\mathbf{d}_\Pi^n - \mathbf{d}_\Pi^{n-1})\|_{0,\Sigma}.
\end{aligned}$$

The last equation in (51) implies that $\boldsymbol{\xi}_h^n - \boldsymbol{\xi}_h^{n-1} = \tau \dot{\boldsymbol{\xi}}_h^n + \tau \dot{\boldsymbol{\xi}}_\Pi^n - \tau(\partial_t \mathbf{d}^n - \partial_\tau \mathbf{d}^n) - \tau \partial_\tau \dot{\boldsymbol{\xi}}_\Pi^n$, which inserted in T_7 gives

$$\begin{aligned}
(57) \quad T_7 &= \tau(\dot{\boldsymbol{\xi}}_h^n - \dot{\boldsymbol{\xi}}_h^{n-1}, \mathbf{L}_h(\mathbf{d}_h^n - \mathbf{d}_h^{n-1}))_\Sigma \\
&= -\tau(\dot{\boldsymbol{\xi}}_h^n - \dot{\boldsymbol{\xi}}_h^{n-1}, \mathbf{L}_h(\boldsymbol{\xi}_h^n - \boldsymbol{\xi}_h^{n-1}))_\Sigma + \tau(\dot{\boldsymbol{\xi}}_h^n - \dot{\boldsymbol{\xi}}_h^{n-1}, \mathbf{L}_h(\mathbf{d}_\Pi^n - \mathbf{d}_\Pi^{n-1}))_\Sigma \\
&= -\tau a^s(\dot{\boldsymbol{\xi}}_h^n - \dot{\boldsymbol{\xi}}_h^{n-1}, \boldsymbol{\xi}_h^n - \boldsymbol{\xi}_h^{n-1}) + \tau(\dot{\boldsymbol{\xi}}_h^n - \dot{\boldsymbol{\xi}}_h^{n-1}, \mathbf{L}_h(\mathbf{d}_\Pi^n - \mathbf{d}_\Pi^{n-1}))_\Sigma \\
&= -\tau^2 a^s(\dot{\boldsymbol{\xi}}_h^n - \dot{\boldsymbol{\xi}}_h^{n-1}, \dot{\boldsymbol{\xi}}_h^n) - \tau^2 a^s(\dot{\boldsymbol{\xi}}_h^n - \dot{\boldsymbol{\xi}}_h^{n-1}, \dot{\boldsymbol{\xi}}_\Pi^n) \\
&\quad + \tau^2 a^s(\dot{\boldsymbol{\xi}}_h^n - \dot{\boldsymbol{\xi}}_h^{n-1}, \partial_t \mathbf{d}^n - \partial_\tau \mathbf{d}^n) + \tau^2 a^s(\dot{\boldsymbol{\xi}}_h^n - \dot{\boldsymbol{\xi}}_h^{n-1}, \partial_\tau \boldsymbol{\xi}_\Pi^n) \\
&\quad + \tau(\dot{\boldsymbol{\xi}}_h^n - \dot{\boldsymbol{\xi}}_h^{n-1}, \mathbf{L}_h(\mathbf{d}_\Pi^n - \mathbf{d}_\Pi^{n-1}))_\Sigma \\
&= -\frac{\tau^2}{2}(\|\dot{\boldsymbol{\xi}}_h^n\|_s^2 - \|\dot{\boldsymbol{\xi}}_h^{n-1}\|_s^2 + \|\dot{\boldsymbol{\xi}}_h^n - \dot{\boldsymbol{\xi}}_h^{n-1}\|_s^2) \\
&\quad + \tau^2 \|\dot{\boldsymbol{\xi}}_h^n - \dot{\boldsymbol{\xi}}_h^{n-1}\|_s \left(\|\dot{\boldsymbol{\xi}}_\Pi^n\|_s + \tau^{1/2} \|\partial_{tt} \mathbf{d}\|_{L^2(t_{n-1}, t_n; H^1(\Sigma)^d)} + \|\partial_\tau \dot{\boldsymbol{\xi}}_\Pi^n\|_s \right) \\
&\quad + \tau \|\dot{\boldsymbol{\xi}}_h^n - \dot{\boldsymbol{\xi}}_h^{n-1}\|_{0,\Sigma} \|\mathbf{L}_h(\mathbf{d}^n - \mathbf{d}^{n-1})\|_{0,\Sigma}.
\end{aligned}$$

The last term can be easily bounded as follows

$$\begin{aligned}
(58) \quad T_8 &= \tau^2(\partial_t \dot{\mathbf{d}}^n - \partial_\tau \dot{\mathbf{d}}^n, \mathbf{L}_h(\mathbf{d}_h^n - \mathbf{d}_h^{n-1}))_\Sigma + \tau^2(\partial_\tau \dot{\boldsymbol{\xi}}_\Pi^n, \mathbf{L}_h(\mathbf{d}_h^n - \mathbf{d}_h^{n-1}))_\Sigma \\
&= -\tau^2 a^s(\partial_t \dot{\mathbf{d}}^n - \partial_\tau \dot{\mathbf{d}}^n, \boldsymbol{\xi}_h^n - \boldsymbol{\xi}_h^{n-1}) - \tau^2 a^s(\partial_\tau \dot{\boldsymbol{\xi}}_\Pi^n, \boldsymbol{\xi}_h^n - \boldsymbol{\xi}_h^{n-1}) \\
&\quad + \tau^2(\partial_t \dot{\mathbf{d}}^n - \partial_\tau \dot{\mathbf{d}}^n, \mathbf{L}_h(\mathbf{d}_\Pi^n - \mathbf{d}_\Pi^{n-1}))_\Sigma + \tau^2(\partial_\tau \dot{\boldsymbol{\xi}}_\Pi^n, \mathbf{L}_h(\mathbf{d}_\Pi^n - \mathbf{d}_\Pi^{n-1}))_\Sigma \\
&\leq \tau^2 \|\boldsymbol{\xi}_h^n - \boldsymbol{\xi}_h^{n-1}\|_s^2 (\|\partial_t \dot{\mathbf{d}}^n - \partial_\tau \dot{\mathbf{d}}^n\|_s + \|\partial_\tau \dot{\boldsymbol{\xi}}_\Pi^n\|_s) \\
&\quad + C \|\mathbf{L}_h(\mathbf{d}^n - \mathbf{d}^{n-1})\|_{0,\Sigma} (\|\partial_t \dot{\mathbf{d}}^n - \partial_\tau \dot{\mathbf{d}}^n\|_{0,\Sigma} + \|\partial_\tau \dot{\boldsymbol{\xi}}_\Pi^n\|_{0,\Sigma}).
\end{aligned}$$

We estimate $\|\mathbf{L}_h(\mathbf{d}^n - \mathbf{d}^{n-1})\|_{0,\Sigma}$ on the right hand side of (56)-(58) using (20) and (41) as follows

$$(59) \quad \|\mathbf{L}_h(\mathbf{d}^n - \mathbf{d}^{n-1})\|_{0,\Sigma} \leq C \|\mathbf{L}(\mathbf{d}^n - \mathbf{d}^{n-1})\|_{0,\Sigma} \leq C \tau^{1/2} \|\partial_t \mathbf{Ld}\|_{L^2(t_{n-1}, t_n; L^2(\Sigma)^d)}.$$

We use Young's inequality in (56)-(58) and insert the resulting relations into (55), which yields

$$\begin{aligned}
& \frac{\rho^f}{2} (\|\boldsymbol{\theta}_h^n\|_{0,\Omega}^2 - \|\boldsymbol{\theta}_h^{n-1}\|_{0,\Omega}^2 + \|\boldsymbol{\theta}_h^n - \boldsymbol{\theta}_h^{n-1}\|_{0,\Omega}^2) + 2\tau\mu K^2 \|\boldsymbol{\theta}_h^n\|_{1,\Omega}^2 + \tau|\phi_h^n|_{s_h} \\
& + \frac{\rho^s \varepsilon}{2} (\|\dot{\boldsymbol{\xi}}_h^n\|_{0,\Sigma}^2 - \|\dot{\boldsymbol{\xi}}_h^{n-1}\|_{0,\Sigma}^2 + \|\dot{\boldsymbol{\xi}}_h^n - \dot{\boldsymbol{\xi}}_h^{n-1}\|_{0,\Sigma}^2) \\
& + \frac{1}{2} (\|\boldsymbol{\xi}_h^n\|_s^2 - \|\boldsymbol{\xi}_h^{n-1}\|_s^2 + \|\boldsymbol{\xi}_h^n - \boldsymbol{\xi}_h^{n-1}\|_s^2) \\
& + \frac{1}{2} \frac{\tau^2}{\rho^s \varepsilon} (\|\mathbf{L}_h \boldsymbol{\xi}_h^n\|_{0,\Sigma}^2 - \|\mathbf{L}_h \boldsymbol{\xi}_h^{n-1}\|_{0,\Sigma}^2 + \|\mathbf{L}_h (\boldsymbol{\xi}_h^n - \boldsymbol{\xi}_h^{n-1})\|_{0,\Sigma}^2) \\
& + \frac{\tau^2}{2} (\|\dot{\boldsymbol{\xi}}_h^n\|_s^2 - \|\dot{\boldsymbol{\xi}}_h^{n-1}\|_s^2 + \|\dot{\boldsymbol{\xi}}_h^n - \dot{\boldsymbol{\xi}}_h^{n-1}\|_s^2) \\
\leq & \frac{\tau \delta_1}{2} (\rho^f \|\boldsymbol{\theta}_h^n\|_{0,\Omega}^2 + \rho^s \varepsilon \|\dot{\boldsymbol{\xi}}_h^n\|_{0,\Sigma}^2 + \|\boldsymbol{\xi}_h^n\|_s^2 + \|\boldsymbol{\theta}_h^n\|_{1,\Omega}^2 + |\phi_h^n|_{s_h}^2 + \frac{\tau^2}{\rho^s \varepsilon} \|\mathbf{L}_h \boldsymbol{\xi}_h^n\|_{0,\Sigma}^2) \\
& + \frac{\delta_1}{2} (\tau^2 \|\dot{\boldsymbol{\xi}}_h^n - \dot{\boldsymbol{\xi}}_h^{n-1}\|_s^2 + \rho^s \varepsilon \|\dot{\boldsymbol{\xi}}_h^n - \dot{\boldsymbol{\xi}}_h^{n-1}\|_{0,\Sigma}^2 + \|\boldsymbol{\xi}_h^n - \boldsymbol{\xi}_h^{n-1}\|_s^2) \\
& + C (\tau^2 \|\partial_{tt} \mathbf{u}\|_{L^2(t_{n-1}, t_n; L^2(\Omega)^d)}^2 + \tau^2 \|\partial_{tt} \dot{\mathbf{d}}\|_{L^2(t_{n-1}, t_n; L^2(\Sigma)^d)}^2 \\
& + \tau^2 \|\partial_{tt} \mathbf{d}\|_{L^2(t_{n-1}, t_n; H^1(\Sigma)^d)}^2 + \tau^5 \|\partial_{tt} \dot{\mathbf{d}}\|_{L^2(t_{n-1}, t_n; H^1(\Sigma)^d)}^2 \\
& + \|\partial_t \boldsymbol{\theta}_\Pi\|_{L^2(t_{n-1}, t_n; L^2(\Omega)^d)}^2 + \|\partial_t \dot{\boldsymbol{\xi}}_\Pi\|_{L^2(t_{n-1}, t_n; L^2(\Sigma)^d)}^2 \\
& + \tau \|\partial_t \boldsymbol{\xi}_\Pi\|_{L^2(t_{n-1}, t_n; L^2(H^1(\Sigma)^d))}^2 + \tau^3 \|\partial_\tau \dot{\boldsymbol{\xi}}_\Pi\|_{L^2(t_{n-1}, t_n; L^2(H^1(\Sigma)^d))}^2 + \tau \|\boldsymbol{\omega}_\Pi^n\|_{\mathbf{A}}^2 \\
& + \tau \|\boldsymbol{\theta}_\Pi^n\|_{1,\Omega}^2 + \tau \|\dot{\boldsymbol{\xi}}_\Pi^n\|_{\frac{1}{2},\Sigma}^2 + \tau^2 \|\partial_t \mathbf{L} \mathbf{d}\|_{L^2(t_{n-1}, t_n; L^2(\Sigma)^d)}^2 + \tau^2 \|\dot{\boldsymbol{\xi}}_\Pi^n\|_s^2).
\end{aligned}$$

The error estimate (49) follows by choosing $\delta_1 = 1/2$, so that the terms in the second bracket on the right hand side can be absorbed into the left hand side, then we sum over n and apply Lemma 1.

Case $r = 2$. Since $\partial_\tau \mathbf{d}_h^n = \dot{\mathbf{d}}_h^n$, we have that

$$\begin{aligned}
\mathbf{d}_h^n - \mathbf{d}_h^{n*} &= \mathbf{d}_h^n - \mathbf{d}_h^{n-1} - \tau \dot{\mathbf{d}}_h^{n-1} = \tau (\partial_\tau \mathbf{d}_h^n - \dot{\mathbf{d}}_h^n) + \tau (\dot{\mathbf{d}}_h^n - \dot{\mathbf{d}}_h^{n-1}) \\
&= \tau (\dot{\mathbf{d}}_\Pi^n - \dot{\mathbf{d}}_\Pi^{n-1}) - \tau (\dot{\boldsymbol{\xi}}_h^n - \dot{\boldsymbol{\xi}}_h^{n-1})
\end{aligned}$$

As done for the first two schemes we analyze the three terms T_i with $i = 6, 7, 8$.

$$\begin{aligned}
(60) \quad T_6 &= \frac{\tau^3}{\rho^s \varepsilon} a^s (\boldsymbol{\xi}_h^n, \dot{\mathbf{d}}_\Pi^n - \dot{\mathbf{d}}_\Pi^{n-1}) - \frac{\tau^3}{\rho^s \varepsilon} a^s (\boldsymbol{\xi}_h^n, \dot{\boldsymbol{\xi}}_h^n - \dot{\boldsymbol{\xi}}_h^{n-1}) \\
&\leq \frac{\tau^3}{\rho^s \varepsilon} \|\boldsymbol{\xi}_h^n\|_s (\|\dot{\mathbf{d}}_\Pi^n - \dot{\mathbf{d}}_\Pi^{n-1}\|_s + \|\dot{\boldsymbol{\xi}}_h^n - \dot{\boldsymbol{\xi}}_h^{n-1}\|_s)
\end{aligned}$$

Taking into account the definition (19), we can write T_7 and T_8 as follows

$$\begin{aligned}
(61) \quad T_7 &= \tau^2 (\dot{\boldsymbol{\xi}}_h^n - \dot{\boldsymbol{\xi}}_h^{n-1}, \mathbf{L}_h (\dot{\mathbf{d}}_\Pi^n - \dot{\mathbf{d}}_\Pi^{n-1}))_\Sigma - \tau^2 a^s (\dot{\boldsymbol{\xi}}_h^n - \dot{\boldsymbol{\xi}}_h^{n-1}, \dot{\boldsymbol{\xi}}_h^n - \dot{\boldsymbol{\xi}}_h^{n-1}) \\
&\leq \tau^2 \|\dot{\boldsymbol{\xi}}_h^n - \dot{\boldsymbol{\xi}}_h^{n-1}\|_{0,\Sigma} \|\mathbf{L}_h (\dot{\mathbf{d}}_\Pi^n - \dot{\mathbf{d}}_\Pi^{n-1})\|_{0,\Sigma} - \tau^2 \|\dot{\boldsymbol{\xi}}_h^n - \dot{\boldsymbol{\xi}}_h^{n-1}\|_{0,\Sigma}^2,
\end{aligned}$$

$$\begin{aligned}
(62) \quad T_8 &= \tau^3 (\partial_t \dot{\mathbf{d}}^n - \partial_\tau \dot{\mathbf{d}}^n, \mathbf{L}_h(\dot{\mathbf{d}}_\Pi^n - \dot{\mathbf{d}}_\Pi^{n-1}))_\Sigma + \tau^3 (\partial_\tau \dot{\boldsymbol{\xi}}_\Pi^n, \mathbf{L}_h(\dot{\mathbf{d}}_\Pi^n - \dot{\mathbf{d}}_\Pi^{n-1}))_\Sigma \\
&\quad - \tau^3 a^s (\partial_t \dot{\mathbf{d}}^n - \partial_\tau \dot{\mathbf{d}}^n, \dot{\boldsymbol{\xi}}_h^n - \dot{\boldsymbol{\xi}}_h^{n-1}) - \tau^3 a^s (\partial_\tau \dot{\boldsymbol{\xi}}_\Pi^n, \dot{\boldsymbol{\xi}}_h^n - \dot{\boldsymbol{\xi}}_h^{n-1}) \\
&\leq \tau^3 (\|\partial_t \dot{\mathbf{d}}^n - \partial_\tau \dot{\mathbf{d}}^n\|_{0,\Sigma} + \|\partial_\tau \dot{\boldsymbol{\xi}}_\Pi^n\|_{0,\Sigma}) \|\mathbf{L}_h(\dot{\mathbf{d}}_\Pi^n - \dot{\mathbf{d}}_\Pi^{n-1})\|_{0,\Sigma} \\
&\quad + \tau^3 (\|\partial_t \dot{\mathbf{d}}^n - \partial_\tau \dot{\mathbf{d}}^n\|_s + \|\partial_\tau \dot{\boldsymbol{\xi}}_\Pi^n\|_s) \|\dot{\boldsymbol{\xi}}_h^n - \dot{\boldsymbol{\xi}}_h^{n-1}\|_s.
\end{aligned}$$

Adding (60)-(62) to (55) and using Young's inequality, we obtain

$$\begin{aligned}
&\frac{\rho^f}{2} (\|\boldsymbol{\theta}_h^n\|_{0,\Omega}^2 - \|\boldsymbol{\theta}_h^{n-1}\|_{0,\Omega}^2 + \|\boldsymbol{\theta}_h^n - \boldsymbol{\theta}_h^{n-1}\|_{0,\Omega}^2) + 2\tau\mu K^2 \|\boldsymbol{\theta}_h^n\|_{1,\Omega}^2 + \tau |\phi_h^n|_{s_h} \\
&\quad + \frac{\rho^s \varepsilon}{2} (\|\dot{\boldsymbol{\xi}}_h^n\|_{0,\Sigma}^2 - \|\dot{\boldsymbol{\xi}}_h^{n-1}\|_{0,\Sigma}^2 + \|\dot{\boldsymbol{\xi}}_h^n - \dot{\boldsymbol{\xi}}_h^{n-1}\|_{0,\Sigma}^2) \\
&\quad + \frac{1}{2} (\|\boldsymbol{\xi}_h^n\|_s^2 - \|\boldsymbol{\xi}_h^{n-1}\|_s^2 + \|\boldsymbol{\xi}_h^n - \boldsymbol{\xi}_h^{n-1}\|_s^2) + \frac{\tau^2}{2} \|\dot{\boldsymbol{\xi}}_h^n - \dot{\boldsymbol{\xi}}_h^{n-1}\|_s^2 \\
&\leq \frac{\tau \delta_1}{2} (\rho^f \|\boldsymbol{\theta}_h^n\|_{0,\Omega}^2 + \rho^s \varepsilon \|\dot{\boldsymbol{\xi}}_h^n\|_{0,\Sigma}^2 + \|\boldsymbol{\xi}_h^n\|_s^2 + \|\boldsymbol{\theta}_h^n\|_{1,\Omega}^2 + |\phi_h^n|_{s_h}^2) \\
&\quad + \frac{\tau^5}{\delta_1 (\rho^s \varepsilon)^2} \|\dot{\boldsymbol{\xi}}_h^n - \dot{\boldsymbol{\xi}}_h^{n-1}\|_s^2 + \frac{\delta_1}{2} \rho^s \varepsilon \|\dot{\boldsymbol{\xi}}_h^n - \dot{\boldsymbol{\xi}}_h^{n-1}\|_{0,\Sigma}^2 \\
&\quad + C \left(\tau^2 \|\partial_{tt} \mathbf{u}\|_{L^2(t_{n-1}, t_n; L^2(\Omega)^d)}^2 + \tau^2 \|\partial_{tt} \dot{\mathbf{d}}\|_{L^2(t_{n-1}, t_n; L^2(\Sigma)^d)}^2 \right. \\
&\quad + \tau^2 \|\partial_{tt} \mathbf{d}\|_{L^2(t_{n-1}, t_n; H^1(\Sigma)^d)}^2 + \|\partial_t \boldsymbol{\theta}_\Pi^n\|_{L^2(t_{n-1}, t_n; L^2(\Omega)^d)}^2 \\
&\quad + \|\partial_t \dot{\boldsymbol{\xi}}_\Pi^n\|_{L^2(t_{n-1}, t_n; L^2(\Sigma)^d)}^2 + \tau^3 \|\partial_t \dot{\boldsymbol{\xi}}_\Pi^n\|_{L^2(t_{n-1}, t_n; H^1(\Sigma)^d)}^2 \\
&\quad + \tau \|\boldsymbol{\omega}_\Pi^n\|_{\boldsymbol{\Lambda}}^2 + \tau \|\boldsymbol{\theta}_\Pi^n\|_{1,\Omega}^2 + \tau \|\dot{\boldsymbol{\xi}}_\Pi^n\|_{\frac{1}{2},\Sigma}^2 \\
&\quad \left. + \tau^5 \|\dot{\mathbf{d}}^n - \dot{\mathbf{d}}^{n-1}\|_s^2 + \tau^4 \|\mathbf{L}_h(\dot{\mathbf{d}}^n - \dot{\mathbf{d}}^{n-1})\|_{0,\Sigma}^2 \right)
\end{aligned}$$

For the last two terms in the above inequality, we use again (41), so that we have

$$\begin{aligned}
\|\dot{\mathbf{d}}^n - \dot{\mathbf{d}}^{n-1}\|_s &\leq \tau^{1/2} \|\partial_t \dot{\mathbf{d}}\|_{L^2(t_{n-1}, t_n; H^1(\Sigma)^d)} \leq \tau^{1/2} \|\partial_{tt} \mathbf{d}\|_{L^2(t_{n-1}, t_n; H^1(\Sigma)^d)}, \\
\|\mathbf{L}_h(\dot{\mathbf{d}}^n - \dot{\mathbf{d}}^{n-1})\|_{0,\Sigma} &\leq C \|\mathbf{L}(\dot{\mathbf{d}}^n - \dot{\mathbf{d}}^{n-1})\|_{0,\Sigma} \leq C \tau^{1/2} \|\partial_t \mathbf{L} \dot{\mathbf{d}}\|_{L^2(t_{n-1}, t_n; L^2(\Sigma)^d)}.
\end{aligned}$$

We choose $\delta_1 = 1/2$ and τ such that $\frac{\tau^3}{(\rho^s \varepsilon)^2} \leq 1$, then the application of Lemma 1 yields the estimate (50). \square

5. NUMERICAL EXPERIMENTS

In this section, we perform numerical tests to check numerically the performances of the schemes reported in Algorithm 3. In particular, we shall consider stability and convergence, and compare the behavior of the proposed splitting schemes with that of the monolithic one. All the numerical tests are performed using the classical 2D benchmark problem of an ellipsoidal structure that evolves to a circular equilibrium position. The fluid domain Ω is the square $[0, 1]^2$ and the initial position of the structure is an ellipse centered at $(0.5, 0.5)$ with the following initial configuration

$$\mathbf{X}_0(s) = \begin{pmatrix} 0.5 + 0.25\sqrt{2} \cos s \\ 0.5 + \frac{0.25}{\sqrt{2}} \sin s \end{pmatrix}, \quad s \in [0, 2\pi].$$

We used the following physical parameters $\rho^f = \rho^s \varepsilon = 1$, $\mu = 1$. Moreover, we assume that the structure is an elastic string with stiffness $\kappa = 2$.

5.1. Stability. The purpose of this paragraph is to illustrate the stability results of Theorem 1. Unconditional stability is obtained for Algorithm 3 with $r = 1$ and conditional stability with $r = 2$. We compare the results with those obtained with the strongly coupled scheme, Algorithm 1, for which unconditional stability has been established in [12].

The model problem consists in the evolution of an ellipsoidal structure toward a circular equilibrium position. The only force that drives the motion is the elastic reaction force to the initial deformation, hence we expect that the energy of the system decreases to a plateau value. In order to check the stability properties of the schemes, we performed long term simulations decreasing the time step while keeping fixed fluid and solid meshes. The fluid mesh is made of 40×40 square elements subdivided into two triangles, whereas the reference configuration of the structure is divided into 40 subintervals.

Figure 2 reports the time evolution of the total energy of the fluid-structure system, namely,

$$\mathbf{E}_h^n := \rho^f \|\mathbf{u}_h^n\|_{0,\Omega}^2 + \rho^s \varepsilon \|\dot{\mathbf{d}}_h^n\|_{0,\Sigma}^2 + \|\mathbf{d}_h^n\|_s^2.$$

The results of the tests are in agreement with the theoretical analysis. We can appreciate energy decreasing for all the used time steps for Algorithm 1 (a) and for the Algorithm 3 with $r = 1$ (b), whereas we see instability for Algorithm 3 with $r = 2$ (c) when the time step is not sufficiently small.

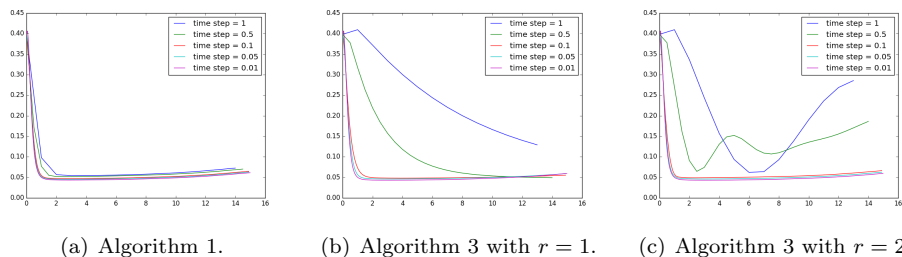


FIGURE 2. Evolution of the total energy \mathbf{E}_h^n for different time-step lengths.

5.2. Convergence. In this paragraph, we numerically investigate the convergence of Algorithms 1 and 3 with respect to the mesh size and to the time-step length. We consider the same model problem as in the previous paragraph, with a different initial configuration of the structure. More precisely, it consists of the static equilibrium of a circular elastic string, centered at the point $(0.5, 0.5)$ with radius 0.25, and immersed in a fluid at rest.

In order to check the convergence rate, we consider as reference solution the one obtained with Algorithm 1 and the following discretization parameters:

$$(63) \quad h_f = h_s = \frac{1}{256}, \quad \tau = 5 \cdot 10^{-5}.$$

Tables 1–3 reports the spatial convergence history for Algorithms 1 and 3, respectively. Here, the time-step length is fixed to $\tau = 0.01$ and errors are evaluated at the final time $t = 0.5$. The three schemes provide practically the same behavior and we observe a sub-optimal rate, which is driven by the regularity of the solution.

TABLE 1. Algorithm 1. Spatial convergence for $\tau = 0.01$.

$h_f = h_s$	1/8	1/16	1/32	1/64	1/128
$\ \mathbf{u}_h^n - \mathbf{u}\ _{0,\Omega}$	7.65E-3	5.92E-3	2.29E-3	8.56E-4	2.94E-4
Rate	–	0.37	1.37	1.42	1.54
$\ \dot{\mathbf{d}}_h^n - \dot{\mathbf{d}}\ _{0,\Sigma}$	5.43E-4	4.29E-4	2.23E-4	1.06E-4	5.93E-5
Rate	–	0.34	0.94	1.07	0.84
$\ \mathbf{d}_h^n - \mathbf{d}\ _s$	3E-02	1.58E-2	8.29E-3	4.69E-3	2.82E-3
Rate	–	0.93	0.93	0.82	0.73

TABLE 2. Algorithm 3 with $r = 1$. Spatial convergence for $\tau = 0.01$.

$h_f = h_s$	1/8	1/16	1/32	1/64	1/128
$\ \mathbf{u}_h^n - \mathbf{u}\ _{0,\Omega}$	7.61E-03	5.91E-3	2.28E-3	8.53E-4	2.91E-4
Rate	–	0.37	1.38	1.42	1.55
$\ \dot{\mathbf{d}}_h^n - \dot{\mathbf{d}}\ _{0,\Sigma}$	5.17E-4	4.15E-4	2.19E-4	1.05E-4	5.91E-5
Rate	–	0.32	0.92	1.05	0.83
$\ \mathbf{d}_h^n - \mathbf{d}\ _s$	2.99E-2	1.57E-2	8.28E-3	4.69E-3	2.82E-3
Rate	–	0.93	0.93	0.82	0.73

TABLE 3. Algorithm 3 with $r = 2$. Spatial convergence for $\tau = 0.01$.

$h_f = h_s$	1/8	1/16	1/32	1/64	1/128
$\ \mathbf{u}_h^n - \mathbf{u}\ _{0,\Omega}$	7.60E-3	5.91E-3	2.28E-3	8.53E-4	2.93E-4
Rate	–	0.36	1.38	1.42	1.54
$\ \dot{\mathbf{d}}_h^n - \dot{\mathbf{d}}\ _{0,\Sigma}$	5.15E-4	4.16E-4	2.19E-4	1.06E-4	5.89E-5
Rate	–	0.31	0.93	1.05	0.84
$\ \mathbf{d}_h^n - \mathbf{d}\ _s$	2.99E-2	1.57E-2	8.28E-3	4.69E-3	2.82E-3
Rate	–	0.93	0.93	0.82	0.73

We test now the convergence rate with respect to the time-step length τ . We ran tests with the following mesh sizes $h_f = h_s = 1/64$, varying the time step as follows: $\tau \in \{1/2^i\}_{i=4\dots 8}$. We compute the errors with respect to a reference solution obtained solving, for each advancing scheme, the problem with $\tau_{ref} = 5E - 05s$ and $h_{ref}^f = h_{ref}^s = 1/64$.

We observe that the partitioned scheme with order two extrapolation results to be stable for sufficiently small values of time step, hence we used values of τ in the stability range. We can observe that the error of the partitioned scheme with order two extrapolation, approaches the value of the monolithic error when the time step reduces properly. This seems to be in agreement with the convergence results in Theorem 2. As far as the order one partitioned scheme, we can see that the rates of convergence appear to be higher. Actually, the error is much higher for big time steps and it is close to the monolithic error for small ones. All the errors have the same behavior as the time step goes to zero as the theory predicts.

TABLE 4. Algorithm 1. Temporal convergence for $h_f = h_s = 1/64$.

τ	1/16	1/32	1/64	1/128	1/256	1/512
$\ \mathbf{u}_h^n - \mathbf{u}\ _{0,\Omega}$	2.65E-6	1.73E-6	1.07E-6	5.96E-7	3.13E-7	1.58E-7
Rate	–	0.61	0.69	0.84	0.93	0.98
$\ \dot{\mathbf{d}}_h^n - \dot{\mathbf{d}}\ _{0,\Sigma}$	6.03E-6	4.07E-6	2.43E-6	1.32E-6	6.86E-7	3.46E-7
Rate	–	0.57	0.74	0.88	0.95	0.99
$\ \mathbf{d}_h^n - \mathbf{d}\ _s$	4.44E-4	2.22E-4	1.11E-4	5.52E-5	2.74E-5	1.35E-5
Rate	–	1.00	1.00	1.00	1.01	1.02

TABLE 5. Algorithm 3 with $r = 1$. Temporal convergence for $h_f = h_s = 1/64$.

τ	1/16	1/32	1/64	1/128	1/256	1/512
$\ \mathbf{u}_h^n - \mathbf{u}\ _{0,\Omega}$	2.40E-4	9.90E-5	3.08E-5	6.86E-6	1.57E-6	4.04E-7
Rate	–	1.28	1.69	2.17	2.12	1.96
$\ \dot{\mathbf{d}}_h^n - \dot{\mathbf{d}}\ _{0,\Sigma}$	1.6E-4	4.36E-5	1.29E-5	3.63E-6	1.11E-6	4.02E-07
Rate	–	1.87	1.75	1.84	1.71	1.46
$\ \mathbf{d}_h^n - \mathbf{d}\ _s$	1.81E-3	1.08E-3	4.37E-4	1.05E-4	3.33E-5	1.42E-5
Rate	–	0.75	1.30	2.06	1.65	1.23

TABLE 6. Algorithm 3 with $r = 2$. Temporal convergence for $h_f = h_s = 1/64$.

τ	1/16	1/32	1/64	1/128	1/256	1/512
$\ \mathbf{u}_h^n - \mathbf{u}\ _{0,\Omega}$	2.21E-4	6.34E-5	4.64E-6	6.39E-7	3.17E-7	1.59E-7
Rate	–	1.81	3.77	2.86	1.01	0.99
$\ \dot{\mathbf{d}}_h^n - \dot{\mathbf{d}}\ _{0,\Sigma}$	8.32E-5	6.06E-5	6.04E-6	1.40E-06	6.83E-7	3.40E-07
Rate	–	0.46	3.33	2.11	1.03	1.01
$\ \mathbf{d}_h^n - \mathbf{d}\ _s$	1.20E-3	6.03E-4	1.26E-4	5.50E-5	2.73E-5	1.35E-05
Rate	–	0.98	2.25	1.20	1.01	1.02

We report the numerical values of the error and the computed convergence rates in Tables 4, 5 and 6. All the schemes provide a rate of converges which is about 1 confirming the theoretical results of Theorem 2.

5.3. Temporal accuracy. In order to illustrate the accuracy of Algorithms 1 and 3, we show the evolution of two nodes on the structure during the simulation relative to the ellipsoidal structure evolving to a circular configuration. At the beginning of the numerical test, the major and minor axes of the ellipse are aligned with the abscissa en coordinate axes, respectively, see Figure 3.

Figures 4 and 5 show the evolutions of the abscissa of A and of the ordinate of B , respectively, for different time-step lengths: $\tau = 0.1, 0.05, 0.01$. The impact of the extrapolation order r on the accuracy of Algorithm 3 is clearly visible with the coarsest discretization. Indeed, for $\tau = 0.1$ we observe that the accuracy of

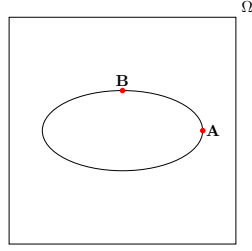


FIGURE 3. Computational domain and interface with the control points A and B .

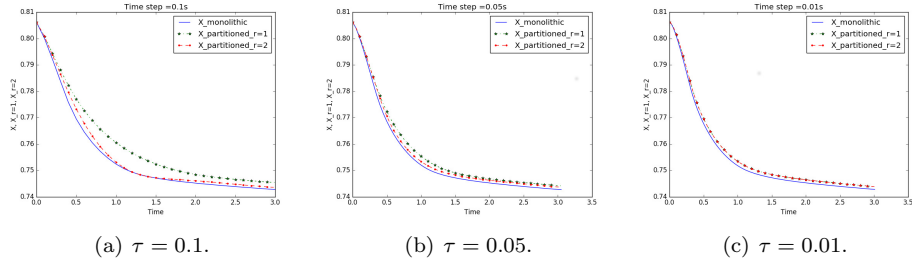


FIGURE 4. Evolution of the abscissa of point A for different time-step lengths.

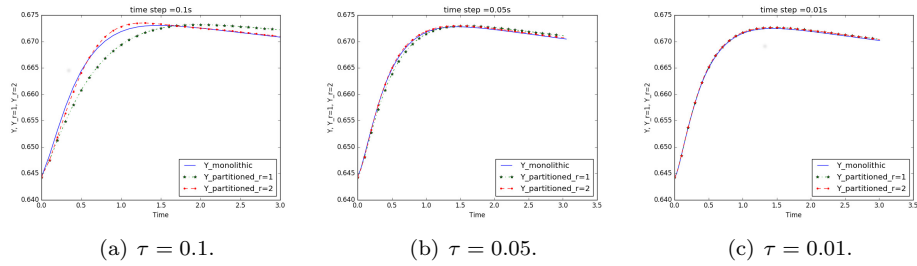


FIGURE 5. Evolution of the ordinate of point B for different time-step lengths.

Algorithm 3 with $r = 2$ is superior to $r = 1$. After time-step refinement, $\tau = 0.05, 0.01$, this difference is negligible and Algorithms 1 and 3 provide very close approximations. These numerical findings are in agreement with relation (22), which shows that Algorithm 3 can be seen as a kinematic perturbation of Algorithm 1. The size of this perturbation depends on both the extrapolation order r and the time-step length τ .

ACKNOWLEDGEMENTS

The third author is member of the INdAM Research group GNCS and her research is partially supported by IMATI/CNR and by PRIN/MIUR.

REFERENCES

- [1] F. Alauzet, B. Fabrèges, M. A. Fernández, and M. Landajuela. Nitsche-XFEM for the coupling of an incompressible fluid with immersed thin-walled structures. *Comput. Methods Appl. Mech. Engrg.*, 301:300–335, 2016.
- [2] F. Alauzet, B. Fabrèges, M.A. Fernández, and M. Landajuela. Nitsche-XFEM for the coupling of an incompressible fluid with immersed thin-walled structures. *Comput. Methods Appl. Mech. Engrg.*, 301:300–335, 2016.
- [3] M. Annese. *Time integration Schemes for Fluid-structure interaction problems: Non-Fitted FEMs For Immersed Thin Structures*. PhD thesis, University of Brescia, PhD Program in Civil and Environmental Engineering, 2017.
- [4] M. Astorino, J.-F. Gerbeau, O. Pantz, and K.-F. Traoré. Fluid-structure interaction and multi-body contact: application to aortic valves. *Comput. Methods Appl. Mech. Engrg.*, 198(45-46):3603–3612, 2009.
- [5] F. Auricchio, D. Boffi, L. Gastaldi, A. Lefieux, and A. Reali. On a fictitious domain method with distributed Lagrange multiplier for interface problems. *Appl. Numer. Math.*, 95:36–50, 2015.
- [6] F. Baaijens. A fictitious domain/mortar element method for fluid-structure interaction. *Int. Jour. Num. Meth. Fluids*, 35:743–761, 2001.
- [7] S. Badia, A. Quaini, and A. Quarteroni. Splitting methods based on algebraic factorization for fluid-structure interaction. *SIAM J. Sci. Comput.*, 30(4):1778–1805, 2008.
- [8] J.W. Banks, W.D. Henshaw, and D.W. Schwendeman. An analysis of a new stable partitioned algorithm for FSI problems. Part II: Incompressible flow and structural shells. *J. Comput. Phys.*, 268:399–416, 2014.
- [9] D. Boffi, F. Brezzi, and M. Fortin. *Mixed finite element methods and applications*, volume 44 of *Springer Series in Computational Mathematics*. Springer, Heidelberg, 2013.
- [10] D. Boffi, N. Cavallini, and L. Gastaldi. Finite element approach to immersed boundary method with different fluid and solid densities. *Math. Models Methods Appl. Sci.*, 21(12):2523–2550, 2011.
- [11] D. Boffi, N. Cavallini, and L. Gastaldi. Finite element approach to immersed boundary method with different fluid and solid densities. *Math. Models Methods Appl. Sci.*, 21(12):2523–2550, 2011.
- [12] D. Boffi, N. Cavallini, and L. Gastaldi. The finite element immersed boundary method with distributed Lagrange multiplier. *SIAM J. Numer. Anal.*, 53(6):2584–2604, 2015.
- [13] D. Boffi and L. Gastaldi. A fictitious domain approach with distributed Lagrange multiplier for fluid-structure interactions. *ArXiv e-prints*, arXiv:1510.06856, 2015.
- [14] D. Boffi and L. Gastaldi. A fictitious domain approach with Lagrange multiplier for fluid-structure interactions. *Numer. Math.*, 135(3):711–732, 2017.
- [15] D. Boffi, L. Gastaldi, and L. Heltai. Numerical stability of the finite element immersed boundary method. *Math. Models Methods Appl. Sci.*, 17(10):1479–1505, 2007.
- [16] D. Boffi, L. Gastaldi, and L. Heltai. On the CFL condition for the finite element immersed boundary method. *Comput. & Structures*, 85(11-14):775–783, 2007.
- [17] Daniele Boffi, Nicola Cavallini, and Lucia Gastaldi. The finite element immersed boundary method with distributed lagrange multiplier. *SIAM Journal on Numerical Analysis*, 53(6):2584–2604, 2015.
- [18] L. Boilevin-Kayl, M. A. Fernández, and J.-F. Gerbeau. A loosely coupled scheme for fictitious domain approximations of fluid-structure interaction problems with immersed thin-walled structures. *SIAM J. Sci. Comput.*, 41(2):B351–B374, 2019.
- [19] L. Boilevin-Kayl, M. A. Fernández, and J.-F. Gerbeau. Numerical methods for immersed FSI with thin-walled structures. *Comput. & Fluids*, 179:744–763, 2019.
- [20] Susanne C. Brenner and L. Ridgway Scott. *The mathematical theory of finite element methods*, volume 15 of *Texts in Applied Mathematics*. Springer, New York, third edition, 2008.

- [21] F. Brezzi and J. Pitkäranta. On the stabilization of finite element approximations of the Stokes equations. In *Efficient solutions of elliptic systems (Kiel, 1984)*, volume 10 of *Notes Numer. Fluid Mech.*, pages 11–19. Friedr. Vieweg, Braunschweig, 1984.
- [22] M. Bukac, C. Canic, R. Glowinski, T. Tambaca, and A. Quaini. Fluid-structure interaction in blood flow capturing non-zero longitudinal structure displacement. *J. Comp. Phys.*, 235(0):515–541, 2013.
- [23] E. Burman and M.A. Fernández. Stabilization of explicit coupling in fluid-structure interaction involving fluid incompressibility. *Comput. Methods Appl. Mech. Engrg.*, 198(5-8):766–784, 2009.
- [24] E. Burman and M.A. Fernández. An unfitted Nitsche method for incompressible fluid-structure interaction using overlapping meshes. *Comput. Methods Appl. Mech. Engrg.*, 279:497–514, 2014.
- [25] H. Casquero, Y. J. Zhang, Bona-Casas. C., L. Dalcin, and H. Gomez. Non-body-fitted fluid-structure interaction: Divergence-conforming b-splines, fully-implicit dynamics, and variational formulation. *Journal of Computational Physics*, 374:625–653, 2018.
- [26] D. Chapelle and A. Ferent. Modeling of the inclusion of a reinforcing sheet within a 3D medium. *Math. Models Methods Appl. Sci.*, 13(4):573–595, 2003.
- [27] J. De Hart, G. W. M. Peters, P. J. G. Schreurs, and F. P. T. Baaijens. A three-dimensional computational analysis of fluid-structure interaction in the aortic valve. *J. Biomech.*, 36(1):103–112, 2003.
- [28] M. Eswaran, U.K. Saha, and D. Maity. Effect of baffles on a partially filled cubic tank: Numerical simulation and experimental validation. *Computers & Structures*, 87(3-4):198–205, 2009.
- [29] M. A. Fernández. Incremental displacement-correction schemes for incompressible fluid-structure interaction. *Numer. Math.*, 123(1):21–65, 2013.
- [30] M. A. Fernández and M. Landajuela. Splitting schemes and unfitted-mesh methods for the coupling of an incompressible fluid with a thin-walled structure. *IMA Journal of Numerical Analysis*, 2019. dry098.
- [31] M. A. Fernández and M. Landajuela. Splitting schemes and unfitted-mesh methods for the coupling of an incompressible fluid with a thin-walled structure. *IMA J. Numer. Anal.*, 40(2):1407–1453, 2020.
- [32] M.A. Fernández. Incremental displacement-correction schemes for incompressible fluid-structure interaction: stability and convergence analysis. *Numer. Math.*, 123(1):21–65, 2013.
- [33] M.A. Fernández, J.F. Gerbeau, and C. Grandmont. A projection semi-implicit scheme for the coupling of an elastic structure with an incompressible fluid. *Int. J. Num. Meth. Engrg.*, 69(4):794–821, 2007.
- [34] M.A. Fernández, M. Landajuela, and M. Vidrascu. Fully decoupled time-marching schemes for incompressible fluid/thin-walled structure interaction. *Journal of Computational Physics*, 297:156–181, 2015.
- [35] M.A. Fernández, J. Mullaert, and M. Vidrascu. Explicit Robin-Neumann schemes for the coupling of incompressible fluids with thin-walled structures. *Comput. Methods Appl. Mech. Engrg.*, 267:566–593, 2013.
- [36] M.A. Fernández, J. Mullaert, and M. Vidrascu. Generalized Robin-Neumann explicit coupling schemes for incompressible fluid-structure interaction: stability analysis and numerics. *Internat. J. Numer. Methods Engrg.*, 101(3):199–229, 2015.
- [37] R. Glowinski, T.-W. Pan, T.I. Hesla, and D.D. Joseph. A distributed Lagrange multiplier/fictitious domain method for particulate flows. *Int. J. of Multiphase Flow*, 25:755–794, 1999.
- [38] G. Guidoboni, R. Glowinski, N. Cavallini, and S. Canic. Stable loosely-coupled-type algorithm for fluid-structure interaction in blood flow. *J. Comp. Phys.*, 228(18):6916–6937, 2009.
- [39] M. Heil and A.L. Hazel. Fluid-structure interaction in internal physiological flows. In *Annual review of fluid mechanics. Volume 43, 2011*, volume 43 of *Annu. Rev. Fluid Mech.*, pages 141–162. Annual Reviews, 2011.
- [40] J. G. Heywood and R. Rannacher. Finite-element approximation of the nonstationary Navier-Stokes problem. IV. Error analysis for second-order time discretization. *SIAM J. Numer. Anal.*, 27(2):353–384, 1990.

- [41] C. Kadapa, W.G. Dettmer, and D. Perić. A stabilised immersed framework on hierarchical b-spline grids for fluid-flexible structure interaction with solid-solid contact. *Comput. Methods Appl. Mech. Engrg.*, 335:472–489, 2018.
- [42] D. Kamensky, M.-C. Hsu, D. Schillinger, J.A. Evans, A. Aggarwal, Y. Bazilevs, M.S. Sacks, and T.J.R. Hughes. An immersogeometric variational framework for fluid–structure interaction: Application to bioprosthetic heart valves. *Comput. Methods Appl. Mech. Engrg.*, 284:1005–1053, 2015.
- [43] Woojin Kim, Injae Lee, and Haecheon Choi. A weak-coupling immersed boundary method for fluidstructure interaction with low density ratio of solid to fluid. *Journal of Computational Physics*, 359:296–311, 2018.
- [44] M. Landajuela, M. Vidrascu, D. Chapelle, and M. A. Fernández. Coupling schemes for the FSI forward predication challenge: comparative study and validation. *Int. J. Numer. Methods Biomed. Eng.*, 33(4):e02813, 23, 2017.
- [45] M. Landajuela, M. Vidrascu, D. Chapelle, and M.A. Fernández. Coupling schemes for the FSI forward prediction challenge: comparative study and validation. *Int. J. Numer. Meth. Biomed. Engng.*, 2016. DOI: 10.1002/cnm.2813.
- [46] M. Lombardi, N. Parolini, A. Quarteroni, and G. Rozza. Numerical simulation of sailing boats: Dynamics, FSI, and shape optimization. In G. Buttazzo and A. Frediani, editors, *Variational Analysis and Aerospace Engineering: Mathematical Challenges for Aerospace Design*, Springer Optimization and Its Applications, pages 339–377. Springer, 2012.
- [47] M. Lukacova-Medvid’ovaa, G. Rusnakovaa, and A. Hundertmark-Zauskovaa. Kinematic splitting algorithm for fluid-structure interaction in hemodynamics. *Comput. Methods Appl. Mech. Engrg.*, 265(1):83–106, 2013.
- [48] U.K. Müller, A. Wasim, E. Fontaine, O. Berg, Y. Cao, D. Lentink, S. Kranenbarg, and J.L. van Leeuwen. Fish and Flag – Exploring Fluid-Structure Interaction during Undulatory Swimming in Fish. In C.T. Lim and J.C.H. Goh, editors, *6th World Congress of Biomechanics (WCB 2010). August 1-6, 2010 Singapore*, volume 31 of *IFMBE Proceedings*, pages 44–47. Springer, 2010.
- [49] E.P. Newren, A.L. Fogelson, R.D. Guy, and R.M. Kirby. Unconditionally stable discretizations of the immersed boundary equations. *J. Comput. Phys.*, 222(2):702–719, 2007.
- [50] M.P. Paidoussis, S.J. Price, and E. de Langre. *Fluid-structure interactions: cross-flow-induced instabilities*. Cambridge University Press, 2011.
- [51] C. S. Peskin. Numerical analysis of blood flow in the heart. *J. Computational Phys.*, 25(3):220–252, 1977.
- [52] C.S. Peskin. The immersed boundary method. *Acta Numer.*, 11:479–517, 2002.
- [53] C. Pozrikidis. *Computational hydrodynamics of capsules and biological cells*. Chapman & Hall/CRC Mathematical and Computational Biology. CRC Press, 2010.
- [54] A. Quaini and A. Quarteroni. A semi-implicit approach for fluid-structure interaction based on an algebraic fractional step method. *Math. Models Methods Appl. Sci.*, 17(6):957–983, 2007.
- [55] J. M. Stockie and B. R. Wetton. Analysis of stiffness in the immersed boundary method and implications for time-stepping schemes. *J. Comput. Phys.*, 154(1):41–64, 1999.
- [56] K. Takizawa and T.E. Tezduyar. Computational methods for parachute fluid-structure interactions. *Arch. Comput. Methods Eng.*, 19:125–169, 2012.
- [57] F.-B. Tian, H. Dai, H. Luo, J.F. Doyle, and B. Rousseau. Fluid-structure interaction involving large deformations: 3D simulations and applications to biological systems. *J. Comput. Phys.*, 258:451–469, 2014.
- [58] C. Tu and C. S. Peskin. Stability and instability in the computation of flows with moving immersed boundaries: a comparison of three methods. *SIAM J. Sci. Statist. Comput.*, 13(6):1361–1376, 1992.

DICATAM, UNIVERSITÀ DEGLI STUDI BRESCIA, 25123 BRESCIA, ITALY
E-mail address: `m.annese@unibs.it`

INRIA, 75012 PARIS, FRANCE AND SORBONNE UNIVERSITÉ AND CNRS, LJLL UMR 7598, 75005
PARIS, FRANCE
E-mail address: `miguel.fernandez@inria.fr`

DICATAM, UNIVERSITÀ DEGLI STUDI DI BRESCIA, 25123 BRESCIA, ITALY
E-mail address: `lucia.gastaldi@unibs.it`
URL: `http://lucia-gastaldi.unibs.it`